Inorganic Chemistry
Cite This: Inorg. Chem. XXXX, XXX, XXX–XXX
Article
pubs.acs.org/IC

Strong Influence of Ancillary Ligands Containing Benzothiazole or Benzimidazole Rings on Cytotoxicity and Photoactivation of Ru(II) Arene Complexes

Matteo Lari,[†,¶] Marta Martínez-Alonso,[†,¶] Natalia Busto,[*,†] Blanca R. Manzano,[‡] Ana M. Rodríguez,[§] M. Isabel Acuña,[⊥] Fernando Domínguez,[⊥] José L. Albasanz,[‡] José M. Leal,[†] Gustavo Espino,[*,†] and Begoña García[*,†]

[†]Departamento de Química, Facultad de Ciencias, Universidad de Burgos, Plaza Misael Bañuelos s/n, 09001 Burgos, Spain
[‡]Departamento de Química Inorgánica, Orgánica y Bioquímica, Facultad de Ciencias y Tecnologías Químicas, IRICA and [§]Departamento de Química Inorgánica, Orgánica y Bioquímica, Escuela Técnica Superior de Ingenieros Industriales, Universidad de Castilla-La Mancha, 13071 Ciudad Real, Spain
[⊥]CIMUS, Universidad de Santiago de Compostela, Avenida Barcelona s/n, 15782 Santiago de Compostela, Spain

Supporting Information

ABSTRACT: A new family of neutral ruthenium(II) arene complexes of the type [Ru(η^6-arene)X(κ^2-*O*,*N*-L)] (η^6-arene = *p*-cym, bz; X = Cl^-, SCN^-; HL1 = 2-(2′-hydroxyphenyl)benzimidazole, HL2 = 2-(2′-hydroxyphenyl)benzothiazole) has been synthesized and characterized. The cytotoxic activity of the Ru(II) complexes was evaluated in several tumor cell lines (A549, HepG2 and SW480) both in the dark and after soft irradiation with UV and blue light. None of the complexes bearing benzimidazole (HL1) as a ligand displayed phototoxicity, whereas the complexes with a benzothiazole ligand (HL2) exhibited photoactivation; the sensitivity observed for UV was higher than for blue light irradiation. The interesting results displayed by HL2 and [Ru(η^6-*p*-cym)(NCS)(κ^2-*O*,*N*-L2)], [**3a**], in terms of photo cytotoxicity prompted us to analyze their interaction with DNA, both in the dark and under irradiation conditions, in an effort to shed some light on their mechanism of action. The results of this study revealed that HL2 interacts with DNA by groove binding, whereas [**3a**] interacts by a dual mode of binding, an external groove binding, and covalent binding of the metal center to the guanine moiety. Interestingly, both HL2 and [**3a**] display a clear preference for AT base pairs, and this causes fluorescence enhancement. Additionally, cleavage of the pUC18 plasmid DNA by the complex is observed upon irradiation. The study of the irradiated form demonstrates that the arene ligand is released to yield species such as [Ru(κ^2-*O*,*N*-L2)(κ^1-*S*-DMSO)$_2$(μ-SCN)]$_2$ [**3c**] and [Ru(κ^2-*O*,*N*-L2)(κ^1-*S*-DMSO)$_3$(SCN)] [**3d**]. Such photo dissociation occurs even in the absence of oxygen and leads to cytotoxicity enhancement, an effect attributed to the presence of [**3d**], thus revealing the potential of [**3a**] as a pro-drug for photoactivated anticancer chemotherapy (PACT).

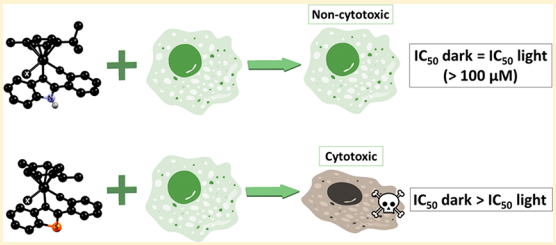

INTRODUCTION

In recent years, the development of new drugs for cancer therapy has become one of the most important research fields. Nowadays, metal complexes with antiproliferative activity are regarded as a promising alternative to conventional organic drugs in anticancer chemotherapy. Platinum complexes, whose cytotoxic activity was discovered serendipitously in 1965 for cisplatin,[1] is the first type of metal compound to be applied in anticancer chemotherapy. Since then, several platinum drugs have been developed as antitumor drugs.[2] However, platinum complexes generally have a number of undesired side effects, a limited range of activity, and a certain degree of tumor resistance.[3] In an effort to overcome such side effects, many research groups have devoted a great deal of effort to the development of new complexes with metal cations other than Pt.[4]

This search has led to the rapid development of ruthenium(III) complexes such as KP1019, which has entered clinical trials.[5] However, Ru(III) pro-drugs are activated by reduction in physiological media,[6] and thus, ruthenium(II) complexes (and especially half-sandwich derivatives) have subsequently aroused the attention of the organometallic chemistry community.[7−9] In particular, the arene moiety stabilizes the lower oxidation state of ruthenium and improves lipophilicity; the chelate ligand confers additional stability by modulating the electronic properties of the metal center, and the monodentate ligand favors activation of the complex by generating a vacant coordination site that allows the binding of biomolecules.[10] Interactions with DNA by forming covalent bonds with nitrogenous bases or reversible interactions (e.g., intercalation) are well-known mechanisms for ruthenium arene complexes and are thought to be responsible for the biological activity of these metal species.[11,12]

Received: August 25, 2018

DOI: 10.1021/acs.inorgchem.8b02299
Inorg. Chem. XXXX, XXX, XXX–XXX

Ruthenium arene derivatives can be easily tuned by changing their structural elements.[13] Benzothiazole[14,15] or benzimidazole[16] derivatives have proved to exhibit antitumor activity. In addition, different arene[17−19] and nonarene[20] ruthenium compounds with ligands containing a benzimidazole or benzothiazole core bound to a 2-pyridine unit or other organic moieties have been reported to exhibit antitumor activity and to have other biological applications.[21−24] Our group has reported an SAR study on a new family of Ru(II) arene complexes of general formula [Ru(η^6-arene)Cl(N∧N)] with aryldiazole ligands and these compounds showed anticancer activity.[25]

Moreover, a selective biological action toward the target cancer cells is highly desired for anticancer metal-drugs. Side effects and systemic toxicity derived from nonselective drugs can preclude their clinical use. Photodynamic therapy (PDT)[26] and photoactivated anticancer chemotherapy (PACT)[27] are well-developed techniques to overcome these drawbacks; the latter technique targets the localized activation of a pro-drug by means of a source of light, with the aim of limiting side effects. Interestingly, many ruthenium complexes exhibit photoactive properties prone to be exploited in anticancer strategies;[28,29] among these, some arene complexes have shown promising photoreactivity.[30,31]

Bearing the above in mind, two different 2-(2′-hydroxyphenyl)-benzazole molecules (see Chart 1) have been used as pro-ligands

Chart 1. Pro-ligands Used in This Work

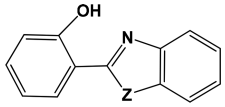

Z = NH, HL1
Z = S, HL2

to obtain ruthenium arene complexes. Recently, semiempirical calculations on HL1 and HL2 have been reported[32] and zinc and copper complexes were synthesized to analyze their luminescent properties[33,34] or their activity toward Alzheimer's disease.[35] However, the antitumor activity of ruthenium complexes with these ligands has not been addressed to date. We report here on a new family of neutral Ru(II) half-sandwich complexes of formula [Ru(η^6-arene)X(N∧O)] with the anionic ligands L1 and L2 (Chart 1).

To analyze the cytotoxicity of these complexes against cancer cells and to establish useful structure−activity relationships, two different arenes (benzene, bz, and *p*-cymene, cym), two leaving groups (Cl^- and SCN^-), and two ancillary ligands that differ only in one group were selected. After deprotonation, the ligands adopt a bidentate chelate coordination mode through the N and O atoms, Ru(N∧O). The cytotoxicity of these complexes was successfully tested in the human tumor cell lines A549 (lung), HepG2 (liver), and SW480 (colon) in the dark and upon irradiation with both UV and blue light. The results obtained revealed the potential of [Ru(η^6-*p*-cym)(NCS)(κ^2-*O*,*N*-L2)] as a photoactivated chemotherapy agent. DNA studies suggest that a dual mode of binding is feasible, namely covalent binding to guanine and groove binding. Moreover, photocleavage of plasmid DNA occurred when an aqueous solution of this complex was irradiated with light, thus transforming the initial complex into a more active derivative.

RESULTS AND DISCUSSION

Synthesis and Characterization of New Ruthenium Complexes. The synthesis of the new half-sandwich Ru(II) chlorido-derivatives of type [Ru(η^6-arene)Cl(O∧N)], [**1a**], [**1b**], [**2a**], and [**2b**], was achieved by reacting overnight at room temperature the appropriate starting dimeric material [RuCl(μ-Cl)(η^6-arene)]$_2$ (arene = *p*-cymene or benzene) with the corresponding pro-ligand (HL1 = 2-(2′-hydroxyphenyl)-1*H*-benzimidazole, HL2 = 2-(2′-hydroxyphenyl)benzothiazole), and triethylamine in methanol or methanol/acetonitrile (see Scheme 1). The Ru(II) isothiocyanato-analogs of general formula [Ru(η^6-arene)(NCS)(L2)] ([**3a**] and [**3b**]) were synthesized by a related protocol, which includes an additional stirring period at 70 °C in the presence of excess KSCN to achieve the Cl^-/SCN^- metathesis reaction. All of the complexes are chiral at the metal site (C_1 symmetry), and thus, they were obtained as racemates (R_{Ru} plus S_{Ru}) in moderate-to-good yields in the form of yellow, orange, or brown powders. The chlorido-derivatives are soluble in common organic solvents, whereas the isothiocyanato derivatives are only sparingly soluble in these solvents (see details in the Synthesis of New Complexes subsection). Interestingly, crystals of complex [**3c**] were obtained from a solution of [**3a**] or [**3b**] in DMSO/acetone.

The new derivatives were fully characterized by spectroscopic and analytical methods. In the cases of [**1a**], [**1b**], [**2a**], and [**3c**], the corresponding crystal structures were solved by X-ray diffraction. Comprehensive assignment of the signals in the NMR spectra was performed from 2D experiments, except for [**3b**] due to its extremely low solubility. In particular, the ^{1}H NMR spectra of all complexes contain signals for the protons of the O∧N ligands, L1 and L2, which, due to OH deprotonation and metal coordination, remain deshielded when compared to those of the free pro-ligands. The [**1a**], [**2a**], and [**3a**] derivatives gave rise to spectroscopic patterns that are compatible with the presence of two diastereotopic methyls and four inequivalent aromatic protons in the *p*-cymene ring, as one would expect for molecules with C_1 symmetry. Moreover, complexes [**1a**] and [**1b**] each display a broad signal in $CDCl_3$ at δ 10.86 and 10.67 ppm, respectively, and this is attributed to the NH group of L1. The ^{1}H−^{1}H NOESY spectra of complex [**1a**] showed exchange peaks between the arene hydrogen atoms $H^2 \leftrightarrow H^6$ and $H^3 \leftrightarrow H^5$, and the methyl groups of the isopropyl unit, which suggest a transient Cl^- decoordination process that involves inversion of the configuration at the Ru center ($R_{Ru} \leftrightarrow S_{Ru}$).[36,37] This process cannot be observed for the benzene derivative [**1b**].

In addition, the ^{13}C{^{1}H} NMR spectra are fully consistent with the molecular structures established by ^{1}H NMR spectroscopy. Interestingly, the chemical shift (δ_C) of the signal for the SCN^- ligand of [**3a**] in DMSO-d_6 is 135 ppm, which suggests the presence of an N-bonded SCN^- ligand according to the literature data,[38] (δ(M-SCN) < 131 ppm < δ(M-NCS)). Moreover, the IR spectrum of [**3a**] shows a strong peak at 2090 cm^{-1} for the C−N stretching frequency, which is also in agreement with a Ru−NCS coordination mode. Typically, wavenumbers higher than 2100 cm^{-1} are assumed to correspond to S-bonded isomers (ν(M−SCN) > 2100 cm^{-1} > ν(M−NCS)).[39−41] For complex [**3b**], we assume the same coordination mode on the basis of its C−N stretching frequency in the IR spectrum, which appears at 2098 cm^{-1}. However, the low solubility of [**3b**] prevented us from confirming this structure by ^{13}C{^{1}H} NMR spectroscopy.

DOI: 10.1021/acs.inorgchem.8b02299
Inorg. Chem. XXXX, XXX, XXX−XXX

Scheme 1. Synthesis of Ruthenium Complexes (Ar = Arene)

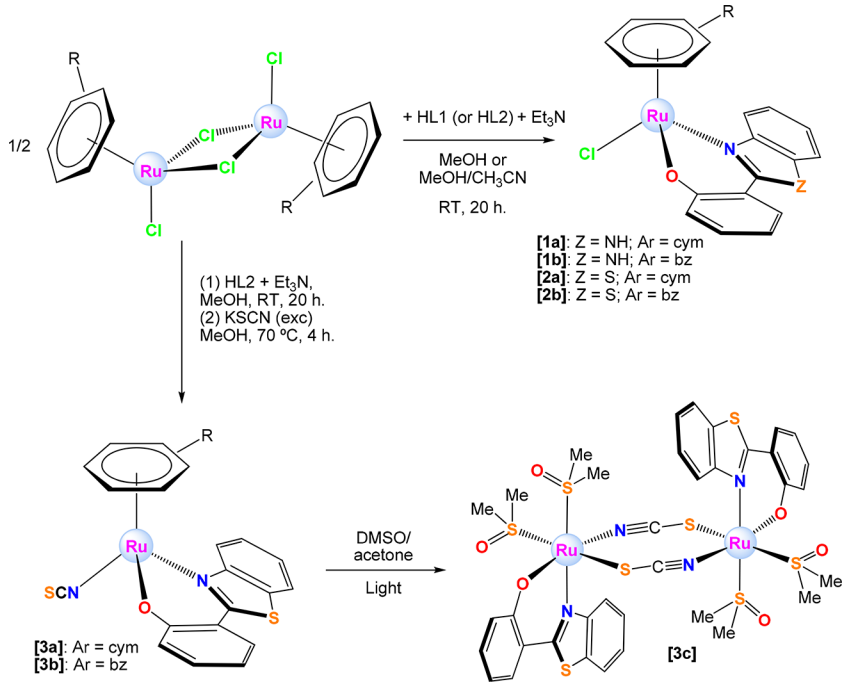

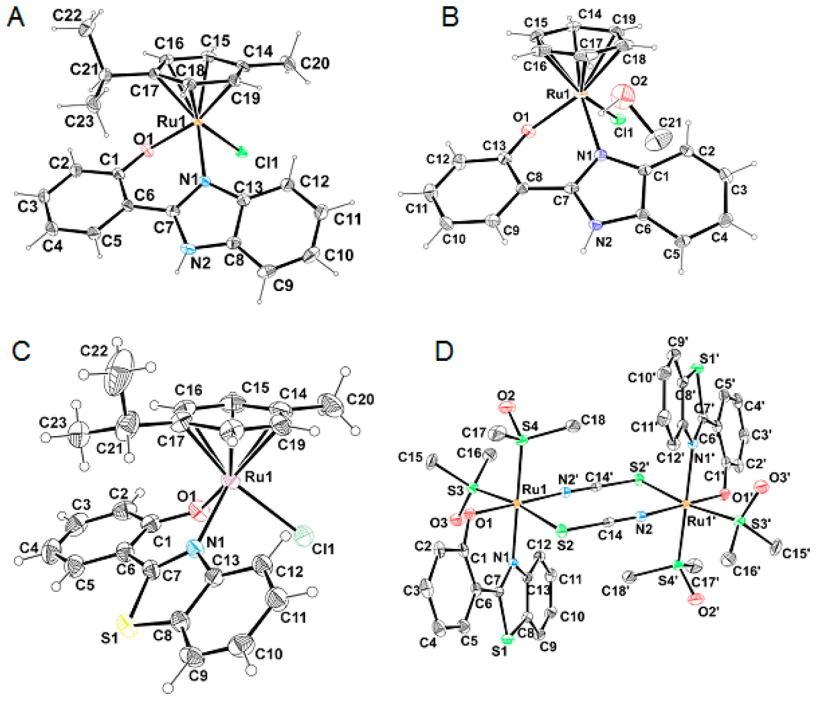

Figure 1. ORTEP diagrams for the molecular structures of (A) [**1a**], (B) [**1b**], (C) [**2a**], and (D) [**3c**] solved by X-ray diffraction. For the sake of clarity, some hydrogen atoms are omitted. Thermal ellipsoids are shown for 30% probability.

The FAB^+ mass spectra contain sets of peaks with m/z values and isotopic distributions that are consistent with the molecular ions, $[M]^+$, as well as with the cationic fragments $[M - Cl]^+$ or $[M - NCS]^+$.

Molar conductivity (Λ_M) measurements were performed at room temperature (20–22 °C) in acetonitrile solution (10^{-3} M) for soluble complexes ([**1a**], [**1b**], [**2a**], and [**3a**]). The Λ_M values are very low (1.9–13.0 S cm^2 mol^{-1}), and this is in agreement with the nonelectrolyte nature of the new complexes.[42]

Solid State Characterization. The molecular and crystal structures of [**1a**], [**1b**]·CH_3OH, [**2a**]·$0.5H_2O$, and [**3c**] were determined by X-ray diffraction. The crystallographic data are given in the Supporting Information (Tables S1–S5), and the corresponding ORTEPs are provided in Figure 1. A selection of bond distances, angles, and other geometric parameters is provided in Table 1 and Table S2. The corresponding unit cells of the mononuclear derivatives [**1a**] and [**2a**] contain the two enantiomers, R_{Ru} and S_{Ru}, stemming from the stereogenic nature of the metal center. By contrast, the unit cell of [**1b**]

DOI: 10.1021/acs.inorgchem.8b02299
Inorg. Chem. XXXX, XXX, XXX–XXX

Table 1. Selected Bond Distances (Å) and Angles (Deg) For Compounds [1a], [1b]·CH_3OH, and [2a]·$0.5H_2O$

distance/angle	[1a]	[1b]·CH_3OH	[2a]·$0.5H_2O$[a]	
Ru1−Cl1	2.4312(8)	2.4289(8)	2.408(12)	2.399(1)
Ru1−N1	2.076(2)	2.086(3)	2.114(3)	2.105(3)
Ru1−O1	2.068(2)	2.069(3)	2.090(2)	2.073(2)
O1−Ru1−N1	83.72(9)	82.86(9)	82.9(1)	83.4(12)
O1−Ru1−Cl1	87.15(6)	87.35(6)	84.8(8)	85.51(8)
N1−Ru1−Cl1	83.89(7)	86.03(6)	85.57(8)	87.37(8)

[a]Values for the two independent molecules found in the unit cell of [2a]·$0.5H_2O$.

only contains the enantiomer S_{Ru}. Indeed, this complex crystallizes in the orthorhombic chiral space group $P2_12_12_1$, suggesting that [1b] has undergone spontaneous chiral resolution upon crystallization from a racemic solution.[43,44] The three metallic congeners adopt the expected half-sandwich three-legged piano-stool geometry, and the arene ring has a π-bonded η^6-coordination mode, whereas the anionic 2-(2′-hydroxyphenyl)benzimidazolate or 2-(2′-hydroxyphenyl)-benzothiazolate ligands assume a bidentate-chelate coordination mode (κ^2-*N*,*O*). A chloride anion occupies the last site in the coordination sphere of Ru(II). The unit cell of [2a] contains two independent molecules (different enantiomers), which differ slightly in their geometric features (Table 1). Moreover, the benzene ring of [1b] exhibits rotational disorder in such a way that two different rotamers are detected in different unit cells.

In all of the structures, the O∧N chelate ring features an envelope conformation. This is a common feature of six-membered metallacycles comprising at least one atom with sp^3 hybridization, that is, the O atom in these complexes. In addition, the aromatic rings of the respective ligands (L1 or L2) did not exhibit coplanarity between each other, with angles between the benzimidazole (or benzothiazole) and hydroxyphenyl planes ranging from 16 to 20°. The Ru-centroid distances fall in a narrow range (1.66−1.67 Å). The Ru−Cl lengths (2.399(1)−2.4312(8) Å) are close to the upper limit of the characteristic range found in the Cambridge Structural Database (CSD), probably owing to the strong σ-donor nature of the chelate anionic ligand, O∧N. Indeed, the Ru−O distances (2.068(2)−2.090(2) Å) are slightly shorter than the Ru−N distances (2.076(2)−2.114(3) Å) in all cases.

The unit cell of [3c] contains six neutral dinuclear units with the formula [Ru(L2)(κ^1-S-DMSO)$_2$(μ-SCN)]$_2$ and all of these units have the ΛΔ configuration, which is the *meso* form. The formation of these dinuclear units from a solution of [3b] in DMSO involves the replacement of the arene with DMSO molecules followed by dimerization through two bridging SCN^- groups in a head-to-tail disposition (μ-SCN, Figure 1). Both of the Ru(II) centers have a distorted octahedral coordination environment. The coordination sphere for each ruthenium atom is completed with a 2-(2′-hydroxyphenyl) benzimidazolate ligand, which adopts a bidentate-chelate coordination mode (N∧O), and two S-bonded dimethyl sulfoxide molecules in a *cis* arrangement. The crystallization of [3c] from a solution of [3b] in DMSO demonstrates the easy loss of the arene moiety and its replacement by S-bonded DMSO molecules. Compound [3c] also crystallized from a DMSO solution of [3a]. A search in the CSD of related crystal structures containing the [Ru(SCN)]$_2$ unit showed only one record for thiocyanato-bridged ruthenium complexes.[45] The Ru−S distances for the thiocyanate (2.487(1) Å) are longer than those for the S-bonded DMSO molecules (2.258(1)−2.265(1) Å). The Ru−N bond distances are 2.035(3) Å (Ru−NCS) and 2.118(3) Å (Ru−N∧O). Lastly, the Ru−O bond distance is 2.047(3) Å. The geometry of the Ru−N−C−S units deviates slightly from linearity since the Ru−N−C angles are 164.3(3)°, that is, below 180°, whereas the SCN angles are 179.6(4)° and the Ru−S−C angles are 104.5(1)°. Moreover, in the eight-membered $Ru_2(SCN)_2$ metallacycle, all of the atoms essentially lie in the same plane. The angle formed between the benzothiazole and hydroxyphenyl planes is 7.5°.

An analysis of the respective 3D crystal structures revealed the presence of $\pi-\pi$ interactions in complexes [1a], [2a], and [3c] involving pairs of ligands L1 or L2 (Table S5). In the case of [1a], this interaction, which extends along the crystallographic *b* axis, is triple and involves the three rings of L1 arranged in a head-to-tail disposition (Figure S1). In the case of [2a], the interaction is established between the ligands of two independent molecules and involves the benzene ring of one ligand and the thiazole ring of the other (Figure S2). In the case of [3c], both L2 ligands of the dinuclear molecule are entangled in $\pi-\pi$ interactions and, in this way, a chain that extends along the crystallographic *a* axis is formed (Figure S3). The interaction is double for every pair of ligands, which are arranged in a head-to-tail disposition, and involves the hydroxyphenyl ring of one ligand and the thiazole ring of the other. Additionally, for [1a], [1b], and [2a], hydrogen bonds involving the chloride anions or oxygen atoms of the complexes are formed. Likewise, the crystal structure of [1b] features one CH_3OH molecule per asymmetric unit, which takes part in hydrogen bonds both as a donor and as an acceptor, with three different ruthenium entities to provide additional stability to the 3D crystal network. Interestingly, in [3c] there is an S-π interaction between the sulfur atom of the thiocyanate bridge and the phenolate ring of the O∧N ligand (see Figure S4 and Table S4, S-centroid = 3.97 Å). This kind of interaction is very common in proteins (e.g., cysteine moieties) and the usual S-centroid distance is 3.9 Å.[46,47]

Cellular Uptake. The cellular uptake of the six synthesized complexes in SW480 cells was evaluated by means of ICP-MS (Figure 2). In light of the gathered results, it is clear that the leaving group has no effect on the ability of these complexes to get into the cells. By contrast, the Ru accumulation inside the cells depends mainly on the ancillary ligand since complexes bearing L2 are more internalized than those with L1, and second, on the arene moiety being the complexes with *p*-cymene two-fold more accumulated than benzene derivatives.

Cytotoxic Activity. The cytotoxicity of the ligands and their complexes, except the insoluble derivative [3b], was investigated toward different human cancer cell lines: A549 (lung carcinoma), HepG2 (liver carcinoma), and SW480 (colon adenocarcinoma) at 24 h of incubation time, both in the dark and upon irradiation. The IC_{50} (μM) values (concentration required to inhibit 50% of the cell growth) obtained in the dark and after

DOI: 10.1021/acs.inorgchem.8b02299
Inorg. Chem. XXXX, XXX, XXX−XXX

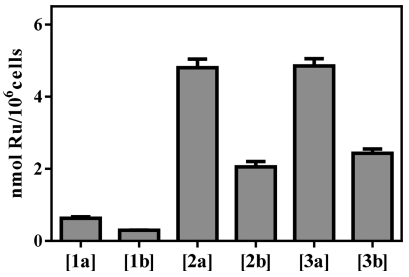

Figure 2. Ruthenium accumulation in SW480 cells treated with 3 μM solutions of the synthesized complexes during 24 h.

soft irradiation with UV (at 365 nm, 20 mW/cm^2 for 5 min) and blue (at 460 nm, 5.5 mW/cm^2 for 20 min) light are listed in Table 2.

HL1 and its derivatives [**1a**] and [**1b**] display negligible cytotoxic activity against the studied tumor cell lines. Although the cytotoxicity displayed by HL2 is low, coordinated to ruthenium it increases sharply, [**2b**] being the most cytotoxic derivative in the dark. The results obtained in the dark point up the influence of the ancillary ligand (S substituent in HL2 versus NH in HL1) as a key factor for cytotoxicity with no significant differences in terms of biological activity as a function of the leaving group.

As to the photo cytotoxicity of the ligands and the metal complexes, the calculated photoindex values (PI) are plotted (Figure 3) for both UV and blue light irradiation in the studied tumor cell lines. Interestingly, none of the complexes bearing benzimidazole as a ligand (HL1) displayed phototoxicity. On the contrary, the complexes with HL2 ligand exhibit certain degree of photo activation under the soft irradiation conditions; the sensitivity observed for UV is higher than for blue light irradiation, [**3a**] being the most active complex against the irradiated tumor cell lines (Figure 3A). As for the ligands, there is no significant irradiation effect on the cytotoxicity of HL1, whereas HL2 is very sensitive to UV irradiation in all the cellular lines studied and its cytotoxicity remains unaltered with blue light irradiation. Figure 3B shows the calculated PI values for both ligands upon UV irradiation.

This interesting result prompted us to analyze the physicochemical properties of complex [**3a**] and its HL2 pro-ligand in solution by studying more in detail this complex with an important DNA biological target.

Physicochemical Properties of HL2 and [3a] in Water. A study of the physicochemical properties and the reactivity of 2-(2′-hydroxyphenyl) benzothiazole (HL2) and [**3a**] was conducted to determine the role played by the ligand in the reactivity of the metal complex.

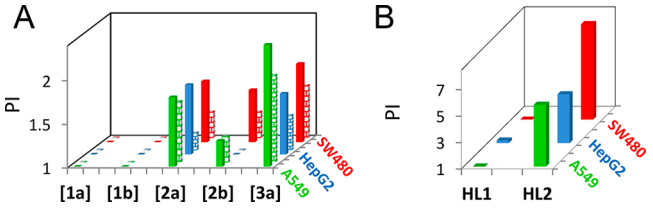

Figure 3. Calculated photoindex (PI = $IC_{50\ dark}/IC_{50\ irr}$) values for the Ru(II) complexes in A549, HepG2, and SW480 cancer cells. (A) Complexes. (B) Ligands. Stuffed bars for UV (5 min, λ = 365 nm, 20 mW/cm^2) and striped bars for blue (20 min, λ = 460 nm, 5.5 mW/cm^2) light irradiation.

HL2 was only poorly soluble (μM concentrations) in buffer solution, I = 6.5 mM ($NaClO_4$), pH = 7.0 and 2% DMSO/H_2O (v:v). The UV−vis absorption spectrum displays two maxima at 288 and 327 nm and a 460 nm band is visible in the emission spectra. Hence, HL2 displays a large Stokes shift of the emission peak (Figure S5). Interestingly, a kinetic process was recorded both in absorbance and fluorescence modes (Figure 4) for concentrations C_L > 3 μM, C_L being the molar concentration of HL2. The well-defined isosbestic points at 272 and 343 nm in the spectral curves denote two species in equilibrium (Figure 4A). Figure 4B shows the evolution with time undergone by the fluorescence spectra; the band at 460 nm gradually vanishes, producing a shoulder, while a new band emerges at 508 nm.

According to the literature,[48] the fluorescence spectrum of the keto-enamine tautomer shows a strong emission band at ∼535 nm and a weak shoulder at 456 nm. This finding demonstrates that the process illustrated in Figure 4B corresponds to the enol-imine to keto-enamine conversion (eq 1) induced by ESIPT (excited state intramolecular proton transfer) effect. It follows that a dual emission occurs from mixtures, with the keto-enamine form emitting at longer wavelengths.

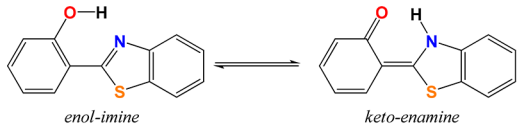

(1)

The contribution of the isomers primarily depends on the DMSO content. Actually, the tracks at 385 nm in the UV−vis absorption spectra (Figure 4A, inset) and at 460 nm in the emission spectra (Figure 4B, inset) reveal that the reaction rate diminishes when the DMSO content increases and becomes very slow above 10% DMSO. The rate constants obtained from fitting of a monoexponential function to the kinetic traces

Table 2. IC_{50} (μM) Values for Ligands HL1 and HL2, Complexes [1a]−[3a], [1b]−[3b], and Cisplatin (CDDP) in Cell Lines A549, HepG2, and SW480 after 24 h Incubation Time, in the Dark and upon Irradiation with UV (5 min, λ = 365 nm, 20 mW/cm^2) or Blue Light (20 min, λ = 460 nm, 5.5 mW/cm^2)

	A549			Hep G2			SW480		
compound	dark	UV	blue	dark	UV	blue	dark	UV	blue
HL1	>100	>100	>100	71.5 ± 2.1	57.8 ± 1.4	67.8 ± 1.4	>100	>100	>100
HL2	87.7 ± 4.2	15.3 ± 1.3	90.2 ± 5.6	80.7 ± 3.1	17.0 ± 1.3	79.0 ± 4.8	>100	12.2 ± 0.7	>100
[**1a**]	>100	>100	>100	>100	>100	>100	>100	>100	>100
[**1b**]	>100	>100	>100	>100	>100	>100	>100	>100	>100
[**2a**]	74.9 ± 5.7	41.8 ± 4.5	43.5 ± 2.9	24.0 ± 1.7	13.7 ± 0.6	20.2 ± 1.0	10.4 ± 1.1	8.3 ± 0.4	6.2 ± 1.0
[**2b**]	16.5 ± 1.2	13.2 ± 1.1	12.3 ± 0.9	4.2 ± 0.2	4.4 ± 0.5	4.8 ± 1.0	7.7 ± 1.1	6.0 ± 0.7	4.9 ± 1.0
[**3a**]	83.1 ± 6.2	41.2 ± 5.3	34.1 ± 2.4	23.8 ± 4.3	13.9 ± 1.3	17.2 ± 3.6	8.7 ± 1.5	5.4 ± 0.7	4.6 ± 0.6
CDDP	46.8 ± 2.3			32.7 ± 1.5			41.2 ± 1.8		

DOI: 10.1021/acs.inorgchem.8b02299
Inorg. Chem. XXXX, XXX, XXX−XXX

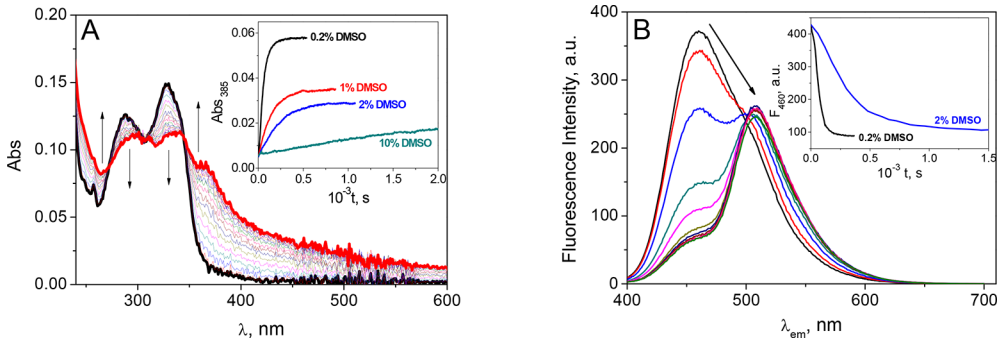

Figure 4. Kinetics of HL2 in buffer solution. (A) Absorbance versus time for the experiment at 0.2% DMSO; inset: track at 385 nm for different DMSO contents. (B) Fluorescence versus time example; inset: track at 460 nm for different DMSO contents. C_L = 10 μM and λ_{exc} = 325 nm.

are 0.0068 s^{-1}, 0.0043 s^{-1}, and 0.00066 s^{-1} at 1, 2, and 10% DMSO, respectively.

In aqueous solution (2% DMSO), $NaClO_4$ and neutral pH, the UV–vis spectra recorded for [**3a**] as a function of time, show first-order kinetic pattern ($k = 4.0 \times 10^{-4}$ s^{-1}, Figure S6A) related to aquation process. In the same conditions, we have observed aquation also for [3b] ($k = 6.5 \times 10^{-4}$ s^{-1}, Figure S6B), but not for the remainder complexes studied. These values resemble aquation processes of other ruthenium complexes.[25] For [**3a**], substitution of SCN- by Cl- was observed in the presence of 4 mM NaCl, with rate constant 1.5×10^{-3} s^{-1}, but aquation of Cl–Ru was not observed. A recent contribution by Sadler[49] reveals that the aqua arene complexes with N∧O chelating ligands are very stable and the kinetics of aquation from the corresponding chlorido complexes are faster than from complexes bearing N∧N ligands. Actually, the observed reaction is put down to SCN^- release and substitution by a H_2O molecule, according to eq 2. From now on, the species formed are denoted as **aqua**-[**3a**]. No kinetics of exchange of SCN^- with DMSO was observed:

$$[(p-\text{cym})\text{RuL2(NCS)}] + H_2O \overset{k}{\rightleftarrows} [(p-\text{cym})\text{RuL2}(OH_2)]^+ + SCN^- \quad (2)$$

Since aqua-complexes are species generally more reactive than their chlorido precursors,[50] the experiments were carried out after completing the aquation of [**3a**].

Acid–Base Behavior of HL2 and Aqua-[3a]. Regarding pH, fluorescence enhancement of HL2 was observed for increasing pH values (Figure S7A). In addition, a notable variation of the absorbance spectra was recorded for different pH values (Figure S7B). The pK_a value obtained by means of the Henderson–Hasselbalch equation,[51] 9.4 ± 0.1, refers to the deprotonation of the phenol group (eq 3). This value concurs with the pK_a obtained for other (hydroxyphenyl) benzothiazoles (for example, for 2-(3′-hydroxyphenyl)-benzothiazole, pK_a = 9.5 and, for 2-(4′-hydroxyphenyl)-benzothiazole pK_a = 8.8).[52]

$$HL2 + H_2O \overset{Ka}{\rightleftarrows} L2^- + H_3O^+ \quad (3)$$

As for **aqua**-[**3a**], the absorbance spectra recorded for increasing pH values show changes and two isosbestic points at 290 and 330 nm (Figure S8), ascribable to formation of the hydroxo-compound [(*p*-cym)Ru(L2)(OH)], according to eq 4. The pK_a′ value 9.2 ± 0.1 obtained from the track at 303 nm (Figure S8, inset) indicates that the complex is present in the aqua form at neutral pH. Similar pK_a values have been reported for formation of some ruthenium hydroxo-compounds.[25] Note that, even though the pK_a values for HL2 and the complex are similar, the acid–base equilibria concern different functional groups, namely the hydroxo group and the leaving water group for HL2 and **aqua**-[**3a**], respectively:

$$[(p-\text{cym})\text{RuL2}(H_2O)]^+ + H_2O \overset{Ka'}{\rightleftarrows} [(p-\text{cym})\text{RuL2(OH)}] + H_3O^+ \quad (4)$$

Below pH = 11, kinetic effects were absent. At pH = 11, a slow kinetic effect (data not shown) was observed; as the new peaks formed are the same as those of the anion ligand form (Figure S7B), we assumed that highly basic conditions can disrupt the binding between the metal and the L2 ancillary ligand.

The prevailing forms for HL2 and **aqua**-[**3a**] were characterized under the buffer conditions used. The cytotoxicity of some organometallic Ru(II) complexes can be ascribed to DNA binding; therefore, to shed some light into the underlying mechanism of the **aqua**-[**3a**]/DNA interaction upon irradiation, we undertook the study of the DNA binding of the HL2 proligand and the **aqua**-[**3a**] complex in the dark.

Interaction of HL2 and Aqua-[3a] with DNA. First, we conducted fluorescence titrations of polynucleotides with HL2. The presence of CT-DNA and poly(dGdC)$_2$ gave rise to a strong red shift in the emission of HL2 ($\Delta\lambda_{em}$ = 55 nm) and, in the presence of poly(dAdT)$_2$, a sudden fluorescence enhancement was also observed (Figure 5A). Since the emission bands centered at 460 and 508 nm are related to the enol-imine and keto-enamine tautomers, respectively, Figure 5A shows that in fresh HL2 solution only the enol tautomer is present. With the addition of DNA, a new band, which corresponds with keto tautomer emission, appears. Actually, Figure 5B shows that the fluorescence enhancement of HL2 is much higher in the presence of the p(dAdT)$_2$ sequence than in the presence of p(dGdC)$_2$ or CT-DNA.

The results provided by fluorometric titrations are endorsed by other complementary techniques. Actually, the HL2/CT-DNA system exhibited a slight decrease both in the circular dichroism bands (Figure S9A) and viscosity measurements (Figure S9B). Moreover, HL2 did not alter the melting temperature of the DNA double-stranded conformation (Figure S9C). These results point out that keto-HL2 tautomer displays selectivity toward AT base-pairs, concurrent with binding to the minor groove.[53,54] Most minor groove binders (netropsin, distamycin, Hoechst 33258, berenil, 40,6-diamidino-2-phenylindole, and SN-6999) are prone to interact with

DOI: 10.1021/acs.inorgchem.8b02299
Inorg. Chem. XXXX, XXX, XXX–XXX

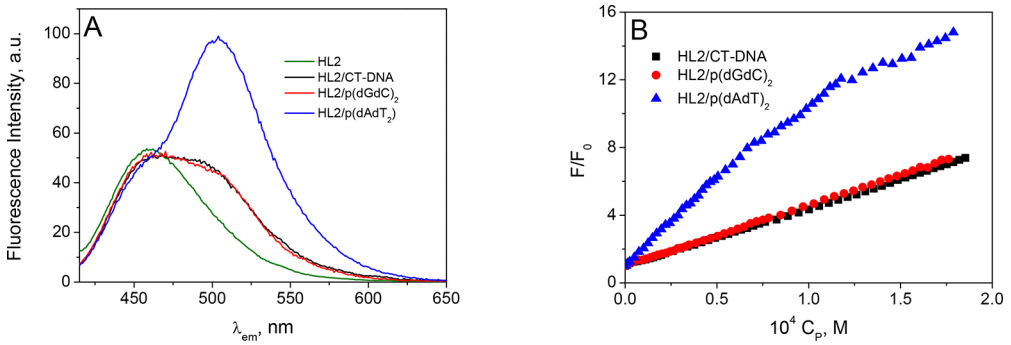

Figure 5. (A) Comparison of the fluorescence spectra of the titration of HL2 with different polynucleotides at $C_P/C_L = 10$. (B) Titration track at λ_{em} = 500 nm for the HL2/p(dAdT)$_2$, HL2/CT-DNA, and HL2/p(dGdC)$_2$ systems; the fluorescence intensity F is divided by F_0, that is, the fluorescence intensity of the free ligand at λ_{em} = 500 nm. C_L = 2.5 μM, C_P = 0–180 μM, and λ_{ex} = 355 nm.

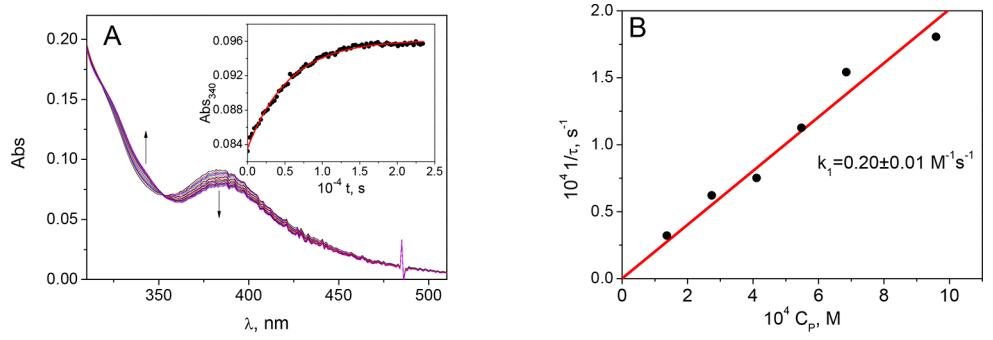

Figure 6. (A) Example of kinetic spectra for the interaction between the **aqua**-[**3a**] complex (D) and *d*GMP (P), C_D = 14 μM, C_P/C_D = 70; inset: track at 345 nm and fitting (red line) by monoexponential function. (B) Fitting of the rate constants by the $1/\tau = k_1C_P$ equation; 2% DMSO, I = 6.5 mM ($NaClO_4$), pH = 7.0 (NaCac), and T = 25.0 °C.

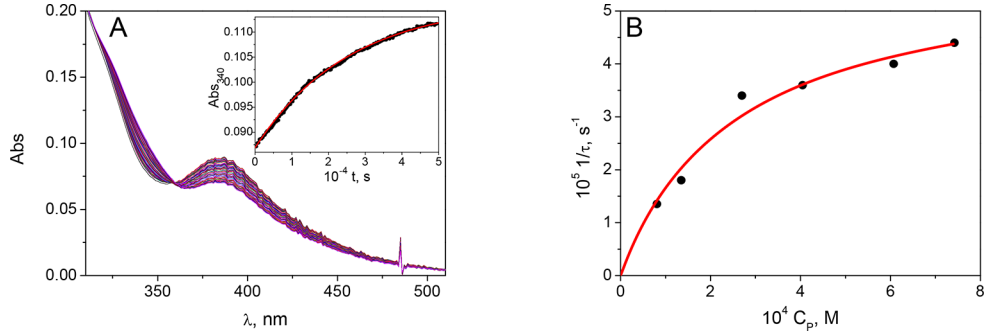

Figure 7. (A) Example of kinetic spectrogram for the interaction between the **aqua**-[**3a**] complex (D) and CT-DNA (P), C_D = 14 μM, C_P/C_D = 45; inset: track at 340 nm. (B) Fitting of eq 6 to the data pairs (red line); 2% DMSO, I = 6.5 mM ($NaClO_4$), pH = 7.0 (NaCac) and T = 25.0 °C.

AT-rich sequences, bringing about only a slight distortion of the double helix.[55]

Concerning the **aqua**-[**3a**] complex, prior to the study of its interaction with DNA, kinetic studies by absorbance measurements were performed in the presence of deoxyadenosine-5′-monophosphate (*d*AMP) and deoxyguanosine-5′-monophosphate (*d*GMP) in excess of nucleotides. No signal variation was detected for **aqua**-[**3a**] with *d*AMP, whereas for the **aqua**-[**3a**]/*d*GMP system a slow kinetic effect was perceptible. The reaction caused hypochromism at 383 nm and a hyperchromic effect at 340 nm in the **aqua**-[**3a**] spectra, with an isosbestic point at 353 nm (Figure 6A). Actually, various ruthenium arene complexes have been reported to bind guanine through the N7 site by substitution of their leaving groups.[56,57]

The time constants ($1/\tau$) increased linearly with the increase in the *d*GMP concentration (C_P) (Figure 6B). In addition, the plot displays close-to-zero intercept, indicating that an irreversible reaction between **aqua**-[**3a**] and *d*GMP is at work, yielding the [**3a**]/*d*GMP complex (eq 5). The slope value provides the reaction rate constant $k_1 = (0.20 \pm 0.01)\ M^{-1}\ s^{-1}$:

$$\textbf{aquo-[3a]} + d\text{GMP} \xrightarrow{k_1} \textbf{[3a]}/d\text{GMP} \qquad (5)$$

We also studied the reaction between **aqua**-[**3a**] and *d*GMP by means of ^{1}H NMR and ^{31}P{^{1}H}-NMR spectroscopy. New sets of peaks emerged in the presence of *d*GMP. In particular, for the [**3a**]/*d*GMP system, a new set of proton peaks was recorded after 3 days, suggesting a slow reaction between the complex and *d*GMP (Figure S10). In addition, a small signal in the ^{31}P NMR spectrum appeared for [**3a**]/*d*GMP (Figure S11). Hence, we can hypothesize the presence of a minor species in which ruthenium is bound to the phosphate group. Moreover,

DOI: 10.1021/acs.inorgchem.8b02299
Inorg. Chem. XXXX, XXX, XXX–XXX

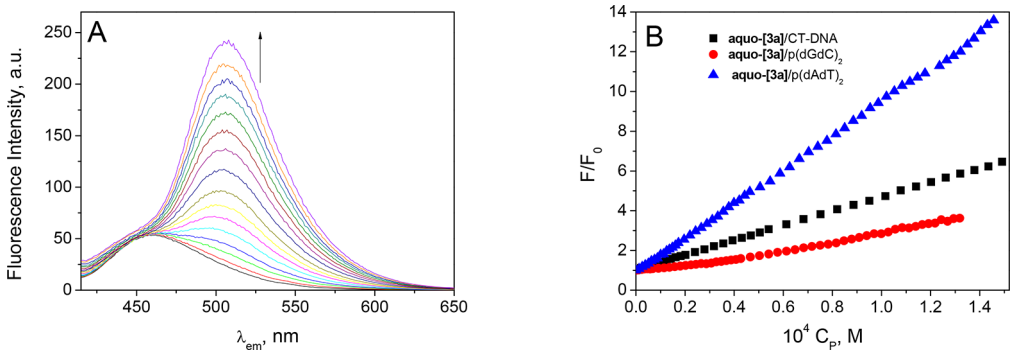

Figure 8. (A) Fluorescence titration of **aqua**-[**3a**] by addition of increasing amounts of CT-DNA (P). (B) Titration track at λ_{em} = 500 nm for the **aqua**-[**3a**]/p(dAdT)$_2$, **aqua**-[**3a**]/CT-DNA, and **aqua**-[**3a**]/p(dGdC)$_2$; the fluorescence intensity F is normalized for the value at λ_{em} = 500 nm of the free complex, F_0. C_D = 2.5 μM, C_P = 0−150 μM, I = 6.5 mM, pH = 7.0, λ_{ex} = 355 nm, 2% DMSO, and T = 25.0 °C.

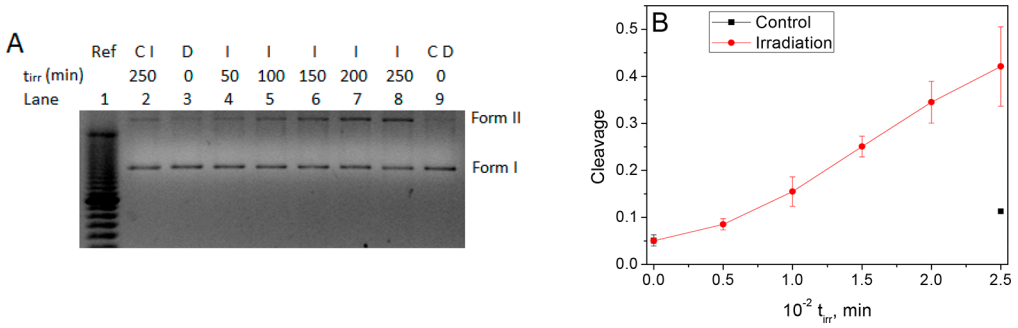

Figure 9. (A) Irradiated **aqua**-[**3a**]/pUC18 samples, I. Lane 1: Molecular weight marker. Lane 2: pUC18 Irradiated control (CI), t_{irr} = 250 min. Lanes 3−8: **aqua**-[**3a**]/pUC18 (I), t_{irr} = 0(D), 50, 100, 150, 200, 250 min. Lane 9: pUC18 Dark Control (CD). C_D = 20 μM, C_P = 20 μM, [$NaClO_4$] = 4.0 mM, [NaCac] = 2.5 mM, pH = 7.0 and λ_{irr} = 325 nm. Incubation at T = 37 °C, overnight. (B) Quantification of the cleavage.

a second more intense peak is ascribed to the major Ru−N species.

Regarding the interaction **aqua**-[**3a**]/CT-DNA, certain variation of the absorbance spectra with time was also observed. Figure 7A shows the spectral kinetic curves, with an isosbestic point at 359 nm. The inset shows the absorbance versus time track at 340 nm. The rate constants ($1/\tau$) were obtained from fitting of a monoexponential function to the data pairs (inset red line).

The spectral changes are similar to those observed for the **aqua**-[**3a**]/*d*GMP system (Figure 6A); hence, a similar interaction with the guanine moiety can be surmised. However, in this case, the increase in the rate constant versus C_P (Figure 7B) is nonlinear, differently from that observed with *d*GMP (Figure 6B). This kinetic behavior agrees well with a fast preassociation mechanism of the metal complex to the nucleic acid via noncovalent binding, which modulates the kinetic rate of the covalent binding to the guanine.[58]

Noncovalent interactions are generally fast, whereas covalent binding to the nitrogenous bases is slower. Therefore, we can assume: (i) the **aqua**-[**3a**] species reacts quickly with CT-DNA to form the noncovalent PD complex, K_1 being the equilibrium constant of this step, and (ii) the PD complex converts into covalent PD* in a second unimolecular, irreversible step, k_2 being the rate-determining constant (eq 6). Bearing this in mind, eq 7 was fitted to the $1/\tau$ versus C_P data-pairs, obtaining the parameters $K_1 = (4 \pm 1) \times 10^3$ M^{-1} and $k_2 = (5.8 \pm 0.5) \times 10^{-5}$ s^{-1}:

$$P + D \underset{\text{fast}}{\overset{K_1}{\rightleftarrows}} PD \xrightarrow[\text{slow}]{k_2} PD^* \qquad (6)$$

$$\frac{1}{\tau} = k_2 \frac{K_1 C_P}{1 + K_1 C_P} \qquad (7)$$

To determine the type of interaction that governs the formation of PD, sets of experiments with freshly prepared solutions were carried out. The fluorometric titration of **aqua**-[**3a**] with CT-DNA (Figure 8) caused a similar fluorescence light-switch and shifted the maximum emission to a wavelength longer than that observed for the HL2/CT-DNA system (Figure 5A). The increase in the emission (or light-switch) in the presence of DNA has been verified for other ruthenium complexes.[59,60] The respective titration experiments of [**3a**] with poly(dAdT)$_2$ and poly(dGdC)$_2$ exhibit preference for AT base-pairs, as observed for the HL2 ligand. Similarly to HL2, few modifications were observed by circular dichroism, viscometry, and melting temperature, agreeing with the minor groove binding hypothesis (Figures S12A−C). These results indicate that the binding of HL2 to the groove promotes the fast interaction observed for **aqua**-[**3a**] to form PD. Groove binding has been verified for other ruthenium arene complexes.[18]

In conclusion, a dual mode of binding of **aqua**-[**3a**] to CT-DNA was observed: fast binding to the minor groove, governed by the ancillary chelating ligand (HL2) to give PD. The groove binding would promote the association of the metal complex to the nucleic acid and then covalent interaction with guanine occurs to give PD* in a two-step mechanism (eq 6). Recently, our group reported a stable bifunctional interaction (covalent and partially intercalated) between the [(η^6-p-cymene)Ru(κ^2-N,N-2-pydaT)]$^{2+}$ fragment and CT-DNA, where both interactions are present concurrently.[61] The difference in the type of the complexes formed with DNA, groove binding for

DOI: 10.1021/acs.inorgchem.8b02299
Inorg. Chem. XXXX, XXX, XXX−XXX

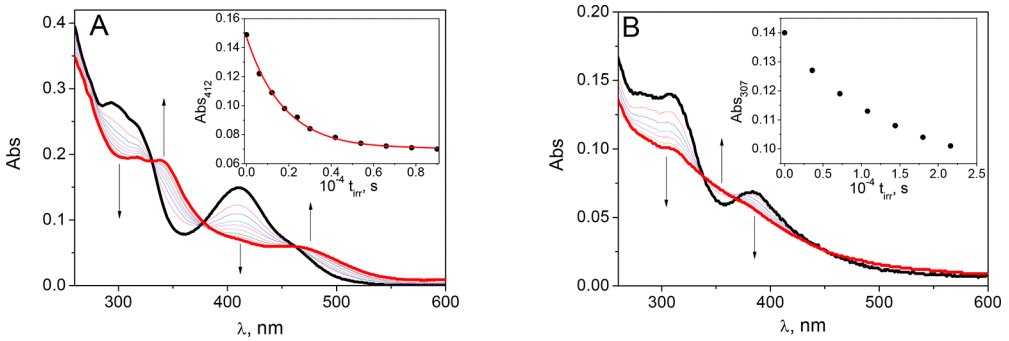

Figure 10. UV−vis absorption kinetics of photorelease of *p*-cymene from the [**3a**] complex in (A) DMSO (Inset: track at 412 nm fitted by a monoexponential curve, $1/\tau = 5.7 \times 10^{-4}$ s^{-1}) and (B) buffer solution (2% DMSO, **aqua**-[**3a**]), I = 6.5 mM ($NaClO_4$), and pH = 7.0 (Inset: Track at 383 nm). C_D = 20 μM, λ_{irr} = 325 nm, and T = 25.0 °C.

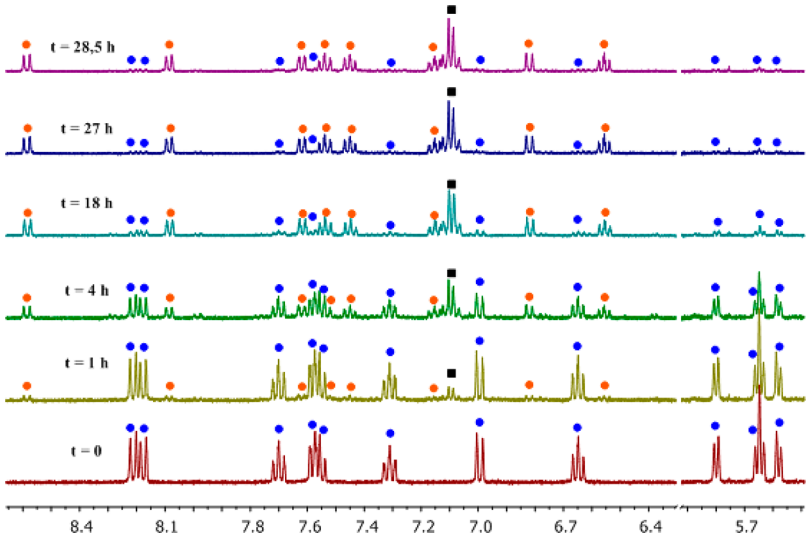

Figure 11. ^{1}H NMR spectra of an irradiated solution of [**3a**] in DMSO-d_6. Blue circle, [**3a**] complex; red circle, [**3d**] complex; black square, free *p*-cymene.

HL2 ligand, and bifunctional binding for **aqua**-[**3a**], has provided a body of evidence about the key role played by the metal regarding DNA interaction due to its ability to bind covalently with the guanine N7 site.

Photoreactivity of Aqua-[3a] Complex. Photo reactivity of the **aqua**-[**3a**] ruthenium complex was evaluated by cleavage of the pUC18 plasmid DNA. The photo cleavage was evaluated by conversion of the plasmid native supercoiled form (Form I) to the circular form (Form II), by means of eq 9 (see Methods subsection). Separation of the different forms was performed by electrophoresis (Figure 9A). Figure 9B shows certain degree of cleavage, which increased with enhancement of the irradiation time at λ = 325 nm.

To assess the oxygen dependence of the DNA cleavage, new photo cleavage experiments were conducted in the presence of scavengers of reactive oxygen species (ROS). Actually, no cleavage decrease was found in the samples containing L-histidine (for $^1O_2$), DMSO (for $OH^\bullet$), and superoxide dismutase (SOD, for O_2^-) (Figure S13). Magennis et al.[62] had reported similar nondependence on oxygen of photo cleavage of the plasmid DNA in the presence of a ruthenium complex (which releases its arene under nitrogen atmosphere).

To properly elucidate if the DNA cleavage is due only to DNA binding of the **aqua**-[**3a**] complex or to changes in the complex upon irradiation, deoxygenated solutions of **aqua**-[**3a**] were irradiated, observing important changes in its absorbance spectra (Figure 10), which suggests alterations in its structure. Furthermore, under the same experimental conditions the kinetic rate is faster in DMSO (Figure 10A) respect to buffer solution (Figure 10B).

The stability of [**3a**] in DMSO-d_6 was monitored by ^{1}H NMR for 3 months under exposure to ambient light and N_2 atmosphere at room temperature. No significant changes were observed after 24 h. However, after 3 months, signals of free *p*-cymene (see Figure S14) and a new set of peaks for a new species, denoted as [**3d**], were detected along with the resonances of [**3a**], which reveals a slow decomposition process that involves arene loss. Moreover, irradiation of a [**3a**] sample in DMSO-d_6 with an arc lamp source of 325 nm speeds up the process in such a way that degradation was completed after 29 h (Figure 11). Again, resonances for free *p*-cymene (labeled with black squares) and a new Ru(II) complex bearing L2 ([**3d**], orange circles) were observed by ^{1}H NMR in the final mixture.

The molecular structure of [**3d**] (Scheme 2) was elucidated by FAB-MS experiments. In particular, the resulting peaks indicate that *p*-cymene was replaced by three DMSO molecules: 470 ([**3d**-2DMSO-d_6]$^+$), 496 ([**3d**-NCS-DMSO-d_6]$^+$), 554 ([**3d**-DMSO-d_6]$^+$), 580 ([**3d**-NCS]$^+$), 638 ([**3d**]$^+$) Da (see spectra in Figures S15−S17). Release of *p*-cymene from

DOI: 10.1021/acs.inorgchem.8b02299
Inorg. Chem. XXXX, XXX, XXX−XXX

Scheme 2. Proposed Photoreaction Found in DMSO Involving Release of *p*-Cymene Ligand

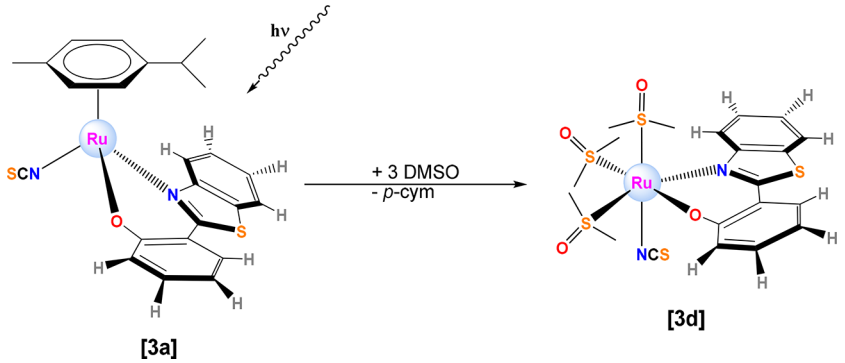

other Ru(II) arene complexes has been reported in previous studies.[63,64]

The photodissociation of the arene and its replacement by solvent molecules leads to labile positions in the coordination sphere of the metal center, which are prone to interact with DNA nucleobases; therefore, we postulate that these interactions could be responsible for the observed photocleavage. Hence, [**3a**] is a potential O_2-independent PACT agent that accomplishes its biological activity through photoinduced dissociation of the arene from the metal center to give [**3d**], which, in turn, would be the actual species responsible for the observed photoactivity. Arene photodissociation has been observed for all the complexes bearing L2 as ancillary ligand (Figure S18), regardless of the arene moiety or leaving group; the metallic products that stem from irradiation are able to cleave plasmid DNA (Figure S19). However, complexes bearing L1 are unable to release the arene moiety after irradiation and cannot cleave DNA. These features confirm arene−photodissociation as the underlying mechanism for the observed photoreactivity. The high cytotoxicity of HL1 in the dark indicates that our future strategy should be based on designing PACT (photo activated chemotherapy) molecules able to release this ligand, that is, chemotherapeutic agents with potential dual activity when both the free ligand (HL1) and the metal fragment exhibit cytotoxic action.[27,65] On the other hand, the high photo cytotoxicity of HL2 can be of interest in the design of photodynamic therapeutic agents.

CONCLUSIONS

We have synthesized and fully characterized a series of new neutral complexes of type [Ru(η^6-arene)X(κ^2*N*,*O*)] using arylbenzazoles as N,O ligands (HL1 = 2-(2′-hydroxyphenyl)-benzimidazole, Z = NH, HL2 = 2-(2′-hydroxyphenyl)-benzothiazole, Z = S). The cytotoxic activity was tested for all the complexes in various cell lines in the dark and after soft irradiation with UV and blue light, revealing that the ancillary ligand (only substituent Z is changed) is a key factor for the observed cytotoxicity. Complexes bearing L1 (Z = NH) are not cytotoxic in the dark or under UV and blue light irradiation. However, complexes bearing L2 as the ancillary ligand (Z = S) are cytotoxic in the dark and can be photoactivated both with UV and blue light. The most interesting results in terms of photoindex, corresponding to [**3a**] complex and HL2 ligand, were studied in depth.

The stability study of complex [**3a**] in DMSO and water revealed the arene loss after irradiation with UV light, even in an oxygen-free atmosphere. This fact confirmed that the process is only and exclusively light-dependent. The observation that **aqua**-[**3a**] is able to interact with DNA also in the dark suggests a complex mechanism for its biological activity, bearing in mind that the observed arene photodissociation can be easily related to the plasmid DNA photo cleavage. Interestingly, DNA cleavage occurs even in the presence of ROS scavengers, confirming an oxygen-independent mechanism. Therefore, these results add interest toward such type of complexes for photoactivation chemotherapy strategies. The possibility of tuning the properties of the complex with arylbenzazoles or adding new ancillary ligands that can promote further interactions could be of interest for new syntheses of PACT (photoactivated chemotherapy) molecules.

MATERIALS AND METHODS

Materials. *Starting Materials.* $RuCl_3 \cdot xH_2O$ was purchased from Apollo Scientific Ltd. and used as received. [(η^6-Arene)Ru(μ-Cl)Cl]$_2$ (arene = *p*-cym or bz,) were prepared according to literature procedures.[66] The ligands 2-(2′-hydroxyphenyl)-1*H*-benzimidazole (HL1) and 2-(2′-hydroxyphenyl)benzothiazole (HL2) were purchased from Aldrich and used without further purification. Deuterated solvents were obtained from SDS and Euriso-top and deaerated by freezing-vacuum cycles and in dry nitrogen atmosphere. Occasionally, some of them were also dried with molecular sieves (MS).

Lyophilized calf thymus (CT) DNA sodium salt was purchased from Sigma-Aldrich. It was dissolved in bidistilled water and sonicated to obtain a mean length of 1000 bp, confirmed by electrophoresis assay. Standardization of stock solutions was performed spectrophotometrically (ε = 13 200 cm^{-1} M^{-1} in bp at λ = 260 nm, I = 0.1 M (NaCl), pH = 7.0, and T = 25.0 °C). Poly(deoxyadenylic-deoxythymidylic) acid sodium salt (p(dAdT)$_2$), and poly-(deoxyguanylic-deoxycytidylic) acid sodium salt (p(dGdC)$_2$) were purchased from Sigma and the concentration was checked by UV−vis spectra, using ε = 13 400 cm^{-1} M^{-1} in base pairs (bp) at λ = 260 nm for p(dAdT)$_2$ and ε = 16 600 cm^{-1} M^{-1} in bp at λ = 254 nm for p(dGdC)$_2$, I = 0.1 M (NaCl), pH = 7.0, and T = 25.0 °C.[67] Plasmid pUC18 (2686 bp) for the photocleavage study was extracted from bacteria and purified by means of a HP Plasmid Midi Kit (OMEGA Biotek, VWR). The concentration of the polynucleotides is always expressed in molarity base pairs, and denoted as C_P. 2′-Deoxyguanosine-5′-monophosphate (5′-*d*GMP) was purchased from Sigma-Aldrich (purity of 99%) and used without further purification. Sodium cacodylate trihydrate ($(CH_3)_2AsOONa \cdot 3H_2O$, NaCac, purity 98%) and sodium perchlorate monohydrate ($NaClO_4 \cdot H_2O$, purity 98%) were purchased from Fluka, and they were just dissolved in water to obtain stock solution. All the experiments between **aqua**-[**3a**] and mono- and polynucleotides were carried out in double distilled water, at a fixed ionic strength (I) and pH. Working solutions had I = 6.5 mM and pH = 7.0.

Methods. All synthetic manipulations were carried out under an atmosphere of dry, oxygen-free nitrogen using standard Schlenk techniques. The solvents were distilled from the appropriate drying agents and degassed before use. Elemental analyses were performed

DOI: 10.1021/acs.inorgchem.8b02299
Inorg. Chem. XXXX, XXX, XXX−XXX

with a LECO CHNS-932 microanalyzer. IR spectra were recorded on a Nicolet Impact 410 (within the frequency range 4000−400 cm^{-1}), and in a Jasco FT/IR-4200 spectrophotometers as KBr pellets. FAB mass spectra (position of the peaks in DA) were recorded with an Autospec spectrometer. The isotopic distribution of the heaviest set of peaks matched very closely that calculated for the formulation of the complex cation in all cases. Conductivity measurements were carried out with a CRISON 522 conductometer, connected to a conductivity cell CRISON 52 92 with platinum electrodes. The solutions of the complexes (10^{-3} M) in acetonitrile (dielectric constant = 36.2 S cm^2 mol^{-1}) were prepared in 5 mL volumetric flasks and measured in test tubes.

NMR samples were prepared under nitrogen atmosphere by dissolving the suitable amount of compound in 0.5 mL of the respective oxygen-free deuterated solvent, and the spectra were recorded at 298 K (unless otherwise stated) on a Varian Unity Inova-400 (399.94 MHz for ^{1}H; 161.9 MHz for ^{31}P; 100.6 MHz for ^{13}C). Typically, 1D ^{1}H NMR spectra were acquired with 32 scans into 32K data points over a spectral width of 16 ppm. ^{1}H and ^{13}C{^{1}H} chemical shifts were internally referenced to tetramethylsilane via 1,4-dioxane in D_2O (δ = 3.75 and 67.19 ppm, respectively) or via the residual ^{1}H and ^{13}C signals of the corresponding solvents according to the values reported by Fulmer et al.[68] Chemical shift values are reported in ppm and coupling constants (J) in hertz. The splitting of proton resonances in the reported ^{1}H NMR data is defined as s = singlet, d = doublet, t = triplet, st = pseudotriplet, q = quartet, sept = septet, m = multiplet, bs = broad singlet. 2D NMR spectra such as ^{1}H−^{1}H gCOSY, ^{1}H−^{1}H NOESY, ^{1}H−^{13}C gHSQC, and ^{1}H−^{13}C gHMBC were recorded using standard pulse sequences. A standard unit calibrated with methanol as a reference controlled the probe temperature (±1 K). All NMR data processing were carried out using MestReNova v10.0.2−15465.

pH Measurements. Desired pH of working solutions was reached by adding small aliquots of concentrated solution of $HClO_4$ and NaOH, using a Metrohm 16 DMS Titrin pH meter, with a glass electrode containing a 3 M KCl solution. The calibration of the instrument was attained through nine buffer solutions.

Spectrophotometric Experiments. UV−vis spectra were recorded by means of a Hewlett-Packard 8453A spectrophotometer (Agilent Technologies), with diode-array detector and coupled with a computer-assisted temperature-control system. Kinetic absorbance study of the interaction between **aqua**-[**3a**] with 5′-dGMP and CT-DNA was performed recording the spectra at a defined time interval and the kinetic curve was treated at a specific wavelength.

Circular Dichroism Equipment. Circular dichroic spectra were recorded with a MOS-450 Bio-Logic dichrograph (Claix, France), at different C_D/C_P ($C_P = 5.0 \times 10^{-5}$ M), C_D, C_P, and L being the analytical concentrations of the complex, ligand, and polynucleotide, respectively. The spectra were recorded from 200 to 600 nm, with an acquisition rate of 0.5 nm s^{-1}.

Viscosity. The elapsed time of 3 mL of DNA solution passing through a capillar was determined in an Ubbelhode microviscometer. Viscosity measurements allows one to determine the elongation of the DNA using eq 8,[69] where t_0, t_1, and t_2 are the elapsed time of the solvent, DNA and complex/DNA solutions ($C_P = 2.0 \times 10^{-4}$ M), respectively. The temperature was kept at 25.0 °C by an external water thermostat:

$$\left(\frac{\eta}{\eta_0}\right)^{1/3} = \left(\frac{t_2 - t_0}{t_1 - t_0}\right)^{1/3} \quad (8)$$

Differential Scanning Calorimetry (DSC). Thermal denaturation study was carried out by means of a Nano-DSC (TA, Waters LLC, New Castle, USA). The working solutions (solutions at different C_D/C_P, $C_P = 4.0 \times 10^{-4}$ M) were degassed before injection in the equipment. The system was pressurized at 3 atm and the solutions were heated from 20 to 110 °C at 1 °C min^{-1} scan rate.

Illumination System. The study of photodissociation was carried out by means of an illuminator. Briefly, it consists of a Xenon short arc lamp (Ushio) coupled with a monochromator. The intensity of the radiation is regulated by means of the power lamp (fixed to 150 W) and the slits of the monochromator. This system was connected with a double beam spectrophotometer Evolution 300 UV−vis (ThermoScientific). The connection allows irradiation of samples at a defined wavelength (λ_{irr}) for a defined time period (t_{irr}) and, then, recording the spectrum. Thus, the kinetics of a photoreaction can be monitored. Moreover, the system was used to irradiate the samples for the photocleavage proofs at different irradiation times and wavelengths.

Cleavage Assay. The separation and detection of the plasmid forms was achieved with an electrophoretic apparatus, coupled with a UV lamp. The solvent was the 1% TBE buffer and the gel 1% TBE containing 1% agarose. After irradiation, the samples were incubated for 14−16 h at 37.0 °C in a KS 4000 I control incubator (IKA) and, then, 10 μL of the solution (Plasmid concentration: 20 μM) was mixed with 2 μL of loading buffer (Bio-Rad, Glycerol 25%) and loaded in the hole. Runs were performed at 5 V/cm for 90 min. To visualize the DNA with the lamp, ethidium bromide was previously added to the gel. Densitometry data were obtained with ImageJ program, and a quantitative value of the cleavage parameter (Cleavage) was obtained through eq 9,[70] where D_I, D_{II}, and D_{III} are the areas of the supercoiled, circular, and linear forms, respectively. For D_I, a correction factor of 1.4 was applied for the decreased ability of the dye to intercalate inside the supercoiled form:[71]

$$\text{Cleavage} = \frac{D_{II} + 2D_{III}}{D_I + D_{II} + 2D_{III}} \quad (9)$$

X-ray Crystallography. Single crystals were obtained by slow evaporation from a [**1b**] solution in methanol and from a [**2a**] solution in methanol/water. As for [**1a**], single crystals were grown by slow diffusion of *n*-hexane into a dichloromethane solution of this complex. In the case of dinuclear complex [**3c**], a monocrystalline sample was achieved from a solution of the parent mononuclear compound [**3b**] in DMSO/acetone as a result of arene/DMSO exchange. A summary of the crystal data collection and refinement parameters for all compounds is given in Table S1 in the Supporting Information. Single crystals of [**1a**], [**1b**]·CH_3OH, [**2a**]·$0.5H_2O$, and [**3c**] were mounted on a glass fiber and transferred to a Bruker X8 APEX II CCD-based diffractometer equipped with a graphite-monochromated Mo Kα radiation source (λ = 0.71073 Å). The highly redundant data sets were integrated using *SAINT*[72] and corrected for Lorentz and polarization effects. The absorption correction was based on the function fitting to the empirical transmission surface as sampled by multiple equivalent measurements with the *SADABS* program.[73] The software package WINGX, version 2014.1,[74] was used for space group determination, structure solution, and refinement by full-matrix least-squares methods based on F^2. A successful solution by direct methods provided most non-H atoms from the E map. The remaining non-H atoms were located in an alternating series of least-squares cycles and difference Fourier maps. All non-H atoms were refined with anisotropic displacement coefficients. Except the N−H for [**1a**] and [**1b**]·CH_3OH, all hydrogen atoms were placed using a "riding model" and included in the refinement at calculated positions. CCDC reference numbers for [**1a**], [**1b**]·CH_3OH, [**2a**]·$0.5H_2O$, and [**3c**] are 1815683, 1815684, 1815685, and 1815686, respectively.

Cellular Uptake. SW480 cells were seeded in 12-well plates (1.5×10^5 cells/well) with DMEM medium supplemented with 10% newborn calf serum and 1% amphotericin−penicillin−streptomycin solution and incubated at 37 °C under 5% CO_2 atmosphere for 24 h. Then cells were exposed to 3 μM of the studied metal complexes during 24 h. Before analysis, cells were washed three times with DPBS (Dulbecco's phosphate buffered saline), then they were harvested. The pellets were resuspended in 1 mL of DPBS and 10 μL was used to count cells by means of an automated cell counter (TC20, BioRad). Then cells were digested for ICP-MS with 65% HNO_3 during 24 h. Finally, solutions were analyzed in a 7700 ICP-MS (Agilent Technologies). Data are reported as the mean ± the standard deviation (n = 3).

MTT Assay. Approximately 1×10^4 of A549, HepG2 or SW480 cells were cultured in 200 μL of culture medium per well (DMEM medium), supplemented with 10% newborn calf serum and 1% amphotericin−penicillin−streptomycin solution in 96-well plates, and

DOI: 10.1021/acs.inorgchem.8b02299
Inorg. Chem. XXXX, XXX, XXX−XXX

incubated at 37 °C under 5% CO_2 atmosphere. Cells were treated with different concentrations of the tested drugs and incubated for 1 h. Then cells were irradiated or not with UV light (at 365 nm, 20 mW/cm^2 for 5 min) and with blue light (at 460 nm, 5.5 mW/cm^2 for 20 min). After 24 h overall incubation, the treatment was retired and cells were incubated with 100 μL of MTT (3-(4,5-dimethyltiazol-2-yl)-2,5-diphenyltetrazolium bromide) (Sigma-Aldrich) dissolved in culture medium (500 μg/mL) for a 3 h further period. At the end of the incubation, the formazan was dissolved by adding 100 μL of solubilizing solution (10%SDS and 0.01 M HCl) to each well. Then plates were incubated at 37 °C with soft agitation. After 18 h, absorbance was read at 590 nm in a microplate reader (Cytation 5 Cell Imaging Multi-Mode Reader, Biotek Instruments, USA). Four replicates per dose were included. The concentrations that produced 50% inhibition of cell viability (IC_{50}) were calculated from MTT data using nonlinear regression of the GraphPadPrism Software Inc. (version 6.01) (USA).

Synthesis of New Complexes. The atom numbering for the ligands and the *p*-cymene ring is reflected in Chart 2.

Chart 2. Atom Numbering

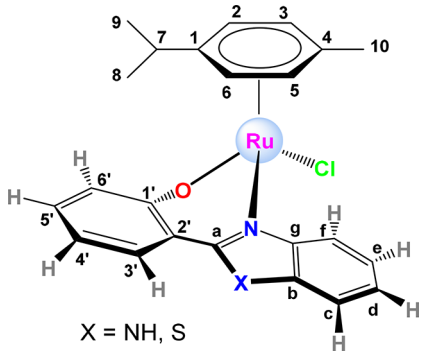

*Synthesis of [(η^6-p-Cymene)RuCl(κ^2-O,N-L1)], **[1a]**.* In a 100 mL Schlenk flask, the ligand 2-(2′-hydroxyphenyl)benzimidazole (0.086 g, 0.409 mmol) was added to a solution of $[RuCl_2(p\text{-cym})]_2$ (0.1251 g, 0.204 mmol) in degassed methanol (10 mL). Et_3N (58 μL, 0.416 mmol) was then added, and the mixture was stirred at room temperature for 20 h and under nitrogen atmosphere. The solution was concentrated, and water was then added to precipitate the product and remove Et_3NHCl. The solid was washed with cold diethyl ether (3 mL). The resulting red−brown powder was dried under vacuum. Yield: 142.8 mg (0.298 mmol, 73%). **M$_r$ ($C_{23}H_{23}ClN_2ORu$)** = 479.9702 g/mol. **Anal. Calc. for $C_{23}H_{23}ClN_2ORu\cdot H_2O$**: C 55.47; H 5.06; N 5.63 **Found**: C 55.13; H 4.99; N 5.98. **^{1}H NMR (400 MHz, $CDCl_3$, 25 °C)** δ 10.67 (s, 1H, H^{N-H}), 7.43 (d, *J* = 8.1 Hz, 1H, H^f), 7.13 (d, *J* = 7.8 Hz, 1H, H^c), 7.01 (d, *J* = 7.6 Hz, 1H, $H^{3'}$), 6.91−6.81 (m, 3H, H^e, $H^{6'}$, $H^{5'}$), 6.63 (t, *J* = 7.5 Hz, 1H, H^d), 6.32 (t, *J* = 6.8 Hz, 1H, $H^{4'}$), 5.38 (d, *J* = 5.8 Hz, 1H, H^3, or H^5), 5.35 (d, *J* = 5.8 Hz, 1H, H^2, or H^6), 5.29 (d, *J* = 5.7 Hz, 1H, H^6, or H^2), 5.20 (d, *J* = 5.7 Hz, 1H, H^5 or H^3), 2.34 (sept, *J* = 6.9 Hz, 1H, H^7), 2.07 (s, 3H, H^{10}), 0.91 (d, *J* = 6.9 Hz, 3H, H^8 or H^9), 0.80 (d, *J* = 6.8 Hz, 3H, H^9 or H^8) ppm. **^{13}C{^{1}H} NMR (101 MHz, $CDCl_3$, 25 °C)** δ 167.3 (s, 1C, $C^{1'}$), 148.2 (s, 1C, C^a), 142.0 (s, 1C, C^g), 133.6 (s, 1C, C^b), 132.0 (s, 1C, $C^{5'}$), 127.3 (s, 1C, $C^{3'}$), 122.8 (s, 1C, C^d), 122.7 (s, 1C, $C^{6'}$), 122.5 (s, 1C, C^e), 117.5 (s, 1C, C^f), 116.0 (s, 1C, $C^{4'}$), 115.9 (s, 1C, $C^{2'}$), 113.3 (s, 1C, C^c), 101.5 (s, 1C, C^1), 97.7 (s, 1C, C^4), 83.0 (s, 1C, C^2 or C^6), 81.8 (s, 1C, C^3 or C^5), 79.9 (s, 1C, C^5 or C^3), 79.8 (s, 1C, C^6 or C^2), 30.5 (s, 1C, C^7), 22.8 (s, 1C, C^8 or C^9), 21.4 (s, 1C, C^9 or C^8), 18.8 (s, 1C, C^{10}) ppm. **FT-IR (KBr, cm^{-1}) selected bands**: 3053 (w, $\nu_{=CH}$), 2961 (w, ν_{-CH}), 1621 (m, ν_{C-N}), 1600 (s, $\nu_{C=C}$), 1532 (m), 1479 (vs, $\nu_{C=N}$), 1459 (s), 1445 (s), 1316 (m), 1261 (s, ν_{C-O}), 1136 (m, $\delta_{N\text{-}Hip}$), 1035 (w), 860 (m), 743 (s, $\delta_{N\text{-}Hoop}$). **MS (FAB+)**: *m*/*z* (%) = 480 (5) ([M]$^+$), 445 (100) ([M-Cl]$^+$). **Molar Conductivity (CH_3CN)**: 11.3 S cm^2 mol^{-1}. **Solubility**: soluble in methanol, dichloromethane, chloroform acetone, and acetonitrile. Partially soluble in water.

*Synthesis of [(η^6-Benzene)RuCl(κ^2-O,N-L1)], **[1b]**.* The synthesis was performed as with [**1a**] in the presence of the ligand 2-(2′-hydroxyphenyl)benzimidazole (0.0843 g, 0.400 mmol), $[RuCl_2(bz)]_2$ (0.0998 g, 0.200 mmol), and Et_3N (58 μL, 0.420 mmol) in methanol/acetonitrile (10:2 mL). Red−brown powder. Yield: 69.1 mg (0.163 mmol, 49%). **M$_r$ ($C_{19}H_{15}ClN_2ORu$)** = 423.8630 g/mol. **Anal. Calc. for $C_{19}H_{15}ClN2ORu\cdot(H_2O)_{1.5}$**: C 50.61; H 4.02; N 6.21. **Found**: C 50.14; H 3.61; N 6,40 **^{1}H NMR (400 MHz, $CDCl_3$, 25 °C)** δ 10.86 (s, 1H, H^{N-H}), 7.56 (d, *J* = 8.4 Hz, 1H, H^f), 7.18 (m, 2H, H^c, $H^{3'}$), 7.04−6.98 (m, 1H, H^e, or $H^{5'}$), 6.94 (m, 2H, $H^{6'}$, H^e, or $H^{5'}$), 6.78 (t, *J* = 7.3 Hz, 1H, H^d), 6.46 (t, *J* = 6.8 Hz, 1H, $H^{4'}$), 5.56 (s, 6H, H^{bz}) ppm. **FT-IR (KBr, cm^{-1}) selected bands**: 3450(w, ν_{N-H}), 3053 (w, $\nu_{=CH}$), 2961 (w, $\nu_{=CH}$), 1621 (m, ν_{C-N}), 1600 (s, $\nu_{C=C}$), 1538 (m), 1479 (vs, $\nu_{C=N}$), 1460 (m), 1445 (m), 1310 (m), 1265 (s, ν_{C-O}), 1139 (m, $\delta_{N\text{-}Hip}$), 1038 (w), 1006 (w), 856 (w), 765 (s, $\delta_{N\text{-}Hoop}$), 750 (s, $\delta_{C\text{-}Hoop}$). **MS (FAB+)**: *m*/*z* (%) = 424 (5) ([M]$^+$), 389 (90) ([M-Cl]$^+$). **Molar Conductivity (CH_3CN)**: 13.0 S cm^2 mol^{-1}. **Solubility**: soluble in methanol, dichloromethane, chloroform, dimethyl sulfoxide, and acetone. Slightly soluble in water.

*Synthesis of [(η^6-p-Cymene)RuCl(κ^2-O,N-L2)], **[2a]**.* The synthesis was performed as with [**1a**] in the presence of the ligand 2-(2′-hydroxyphenyl)benzothiazole (0.0743 g, 0.327 mmol), $[RuCl_2(p\text{-cym})]_2$ (0.0999 g, 0.163 mmol), and Et_3N (48 μL, 0.347 mmol) in methanol (10 mL). Yellow−orange powder. Yield: 85 mg (0.171 mmol, 52%). **M$_r$ ($C_{23}H_{22}ClNORuS$)** = 497.0216 g/mol. **Anal. Calc. for $C_{23}H_{22}ClNORuS\cdot(H_2O)_{0.5}$**: C 54.59; H 4.58; N 2.77; S 6.34 **Found**: C 54.79; H 4.42; N 3.19; S 5.79. **^{1}H NMR (400 MHz, $CDCl_3$, 25 °C)** δ 8.47 (d, *J* = 8.4 Hz, 1H, H^f), 7.78 (dd, *J* = 8.0, 0.6 Hz, 1H, H^c), 7.54 (ddd, *J* = 8.4, 7.3, 1.2 Hz, 1H, H^e), 7.49 (dd, *J* = 7.9, 1.7 Hz, 1H, $H^{3'}$), 7.39 (m, 1H, H^d), 7.26 (m, 1H, $H^{5'}$), 7.18 (dd, *J* = 8.5, 1.2 Hz, 1H, $H^{6'}$), 6.60 (ddd, *J* = 8.0, 6.9, 1.2 Hz, 1H, $H^{4'}$), 5.49 (d, *J* = 6.0 Hz, 1H, H^2, or H^6), 5.33 (d, *J* = 5.9 Hz, 1H, H^2, or H^6), 5.30 (d, *J* = 5.8 Hz, 1H, H^3, or H^5), 5.23 (d, *J* = 5.6 Hz, 1H, H^3, or H^5), 2.68 (sept, *J* = 6.9 Hz, 1H, H^7), 2.04 (s, 3H, H^{10}), 1.14 (d, *J* = 6.9 Hz, 3H, H^8, or H^9), 1.10 (d, *J* = 6.9 Hz, 3H, H^8, or H^9) ppm. **^{13}C{^{1}H} NMR (101 MHz, $CDCl_3$, 25 °C)** δ 169.5 (s, 1C, $C^{1'}$), 166.9 (s, 1C, C^a), 153.1 (s1C, C^g), 134.0 (s, 1C, $C^{5'}$), 131.7 (s, 1C, C^b), 129.6 (s, 1C, $C^{3'}$), 127.1 (s, 1C, C^e), 125.5 (s, 2C, C^f, C^d), 124.4 (s, 1C, $C^{6'}$), 121.5 (s, 1C, C^c), 121.3 (s, 1C, $C^{2'}$), 116.1 (s, 1C, $C^{4'}$), 103.3 (s, 1C, C^1 o C^4), 97.5 (s, 1C, C^1 o C^4), 83.0 (s), 81.24 (s), 81.1 (s), 80.60 (s), 30.9 (s, 1C, C^7), 23.1 (s, 1C, C^8 or C^9), 21.6 (s, 1C, C^8 or C^9), 18.8 (s, 1C, C^{10}) ppm. **FT-IR (KBr, cm^{-1}) selected bands**: 3033 (m, $\nu_{=CH}$), 2958 (w, ν_{-CH}), 1597 (s, ν_{C-N}), 1540 (s, $\nu_{C=C}$), 1491 (vs, $\nu_{C=N}$), 1463 (s), 1441 (s), 1420 (m), 1332 (s), 1213 (s, ν_{C-O}), 1153 (s, $\nu_{C=S}$), 1128 (w), 1033 (w), 875 (w), 832 (w), 753 (s, $\delta_{C\text{-}Hoop}$). **MS (FAB+)**: *m*/*z* (%) = 497 (14) ([M]$^+$), 462 (61) ([M-Cl]$^+$). **Molar Conductivity (CH_3CN)**: 3.4 S cm^2 mol^{-1}. **Solubility**: soluble in acetone, dichloromethane, chloroform, methanol, and acetonitrile and partially soluble in ethanol; slightly soluble in water.

*Synthesis of [(η^6-Benzene)RuCl(κ^2-O,N-L2)], **[2b]**.* The synthesis was performed as with [**1a**] in the presence of the ligand 2-(2′-hydroxyphenyl)benzothiazole (0.0913 g, 0.402 mmol), $[RuCl_2(bz)]_2$ (0.1001 g, 0.200 mmol), and Et_3N (58 μL, 0.420 mmol) in methanol/acetonitrile (8:2 mL). Yellow powder. Yield: 134.6 mg (0.305 mmol, 77%). **M$_r$ ($C_{19}H_{14}ClNORuS$)** = 440.9144 g/mol. **Anal. Calc. for $C_{19}H_{14}ClNORuS\cdot H_2O$**: C 50.17; H 3.37; N 3.52; S 6.57 **Found**: C 49.73; H 3.51; N 3.05; S 6.99. **^{1}H NMR (400 MHz, $CDCl_3$, 25 °C)** δ 8.53 (d, *J* = 8.3 Hz, 1H, H^f), 7.80 (d, *J* = 8.0 Hz, 1H, H^c), 7.57 (t, *J* = 7.7 Hz, 1H, H^e), 7.50 (d, *J* = 7.8 Hz, 1H, $H^{3'}$), 7.42 (t, *J* = 7.6 Hz, 1H, H^d), 7.33−7.27 (m, 1H, $H^{5'}$), 7.24 (d, *J* = 8.2 Hz, 1H, $H^{6'}$), 6.64 (t, *J* = 7.2 Hz, 1H, $H^{4'}$), 5.63 (s, 6H, H^{bz}) ppm. **^{13}C{^{1}H} NMR (101 MHz, $CDCl_3$, 25 °C)** δ 169.9 (s, 1C, $C^{1'}$), 167.4 (s, 1C, C^a), 152.9 (s, 1C, C^g), 134.3 (s, 1C, $C^{5'}$), 131.8 (s, 1C, C^b), 129.6 (s, 1C, $C^{3'}$), 127.4 (s, 1C, C^e), 125.6 (s, 1C, C^d), 125.2 (s, 1C, C^f), 123.7 (s, 1C, $C^{6'}$), 121.9 (s, 1C, $C^{2'}$), 121.6 (s, 1C, C^c), 116.5 (s, 1C, $C^{4'}$), 83.7 (s, 6C, C^{bz}) ppm. **FT-IR (KBr, cm^{-1}) selected bands**: 3056 (w), 3038 (w, $\nu_{=CH}$), 3006 (w, $\nu_{=CH}$), 1599 (s, ν_{C-N}), 1545 (m, $\nu_{C=C}$), 1489 (vs, $\nu_{C=N}$), 1467 (s), 1440 (s), 1420 (m), 1336 (m), 1217 (s, ν_{C-O}), 1155 (m, $\nu_{C=S}$), 1125 (w), 1036 (w), 832 (w), 753−748

DOI: 10.1021/acs.inorgchem.8b02299
Inorg. Chem. XXXX, XXX, XXX−XXX

(s, $\delta_{C\text{-}Hoop}$), 723 (m). **MS (FAB+)**: m/z (%) = 406 (10) ([M-Cl]$^+$). **Molar Conductivity**: It could not be measured due to their poor solubility both water and acetonitrile. **Solubility**: soluble in methanol, dichloromethane, chloroform; partially soluble in acetone and slightly soluble in water and acetonitrile.

Synthesis of [(η^6-p-Cymene)Ru(NCS)(κ^2-O,N-L2)], [3a]. In a 100 mL Schlenk flask, the ligand 2-(2′-hydroxyphenyl)benzothiazole (0.0744 g, 0.327 mmol) was added to a solution of $[RuCl_2(cym)]_2$ (0.1000 g, 0.163 mmol) in degassed methanol (8 mL). Et_3N (48 μL, 0.345 mmol) was then added, and the mixture was stirred at room temperature for 20 h and under nitrogen atmosphere. KSCN (0.0513 g, 0.528 mmol) was added to the mixture and heated at 70 °C for 4 h. The precipitate was filtered and water was added to remove salts. After filtering, the residue was washed with diethyl ether (3 mL). The resulting orange powder was dried under vacuum. Yield: 133.8 mg (0.257 mmol, 79%). **M$_r$ ($C_{24}H_{22}N_2ORuS_2$)** = 519.6526 g/mol. **Anal. Calc. for $C_{24}H_{22}N_2ORuS_2{\cdot}H_2O$**: C 53.79; H 4.01; N 5.68; S 12.16 **Found**: C 53.61; H 4.50; N 5.21; S 11.93. **^{1}H NMR (400 MHz, CD_3CN, 25 °C)** δ 8.25 (d, J = 8.4, 1.1, 0.7 Hz, 1H, H^f), 8.01 (ddd, J = 8.0, 1.2, 0.6 Hz, 1H, H^c), 7.69 (ddd, J = 8.5, 7.2, 1.3 Hz, 1H, H^e), 7.63−7.56 (m, 1H, H$^{3'}$), 7.54 (ddd, J = 8.1, 7.2, 1.1 Hz, 1H, H^d), 7.33 (ddd, J = 8.4, 7.0, 1.7 Hz, 1H, H$^{5'}$), 7.11−7.00 (m, 1H, H$^{6'}$), 6.67 (ddd, J = 7.9, 7.0, 1.2 Hz, 1H, H$^{4'}$), 5.66 (d, J = 5.9 Hz, 1H, H^2, or H^6), 5.54 (d, J = 5.3 Hz, 1H, H^2, or H^6), 5.43 (d, J = 6.1 Hz, 1H, H^3, or H^5), 5.37 (d, J = 6.0 Hz, 1H, H^3, or H^5), 2.69−2.56 (m, 1H, H^7), 1.85 (s, 3H, H^{10}), 1.16 (s, 3H, H^8, or H^9), 1.14 (s, 3H, H^8, or H^9). **^{1}H NMR (400 MHz, DMSO-d_6, 25 °C)** δ 8.21 (d, J = 8.1 Hz, 1H, H^f), 8.17 (d, J = 8.0 Hz, 1H, H^c), 7.70 (t, J = 7.8 Hz, 1H, H^e), 7.58 (d, J = 6.7 Hz, 1H, H$^{3'}$), 7.55 (t, J = 6.3 Hz, 1H, H^d), 7.31 (t, J = 7.7 Hz, 1H, H$^{5'}$), 6.99 (d, J = 8.4 Hz, 1H, H$^{6'}$), 6.65 (t, J = 7.4 Hz, 1H, H$^{4'}$), 5.80 (d, J = 5.9 Hz, 1H, H^2, or H^6), 5.65 (t, J = 6.1 Hz, 2H, H^6 or H^2, H^3, or H^5), 5.58 (d, J = 6.0 Hz, 1H, H^5, or H^3), 1.89 (s, 3H, H^{10}), 1.09 (d, J = 3.5 Hz, 3H, H^8, or H^9), 1.07 (d, J = 3.5 Hz, 3H, H^9, or H^8) ppm. H^7 is overlapped into the residual DMSO signal. **^{13}C{^{1}H} NMR (101 MHz, CD_3CN, 25 °C)** δ 147.0 (s, 1C, C$^{1'}$ or C^a), 145.6 (s, 1C, C$^{1'}$ or C^a), 141.5 (s, 1C), 140.6 (s, 1C), 135.1 (s, 1C), 130.8 (s, 1C), 128.5 (s, 1C), 126.8 (s, 1C), 125.3 (s, 1C), 124.3 (s, 1C), 123.2 (s, 1C), 117.2 (s, 1C), 105.4 (s, 1C), 99.6 (s, 1C), 84.4 (s, 1C), 83.7 (s, 1C), 83.4 (s, 1C), 82.6 (s, 1C), 31.9 (s, 1C, C^7), 22.8 (s, 1C, C^8 or C^9), 21.8 (s, 1C, C^8 or C^9), 18.8 (s, 1C, C^{10}). **^{13}C{^{1}H} NMR (101 MHz, DMSO-d_6, 25 °C)** δ 168.4 (s, 1C, C$^{1'}$), 166.4 (s, 1C, C^a), 152.1 (s, 1C, C^g), 135.4 (s, 1C, C^{SCN}), 134.1 (s, 1C, C$^{5'}$), 131.0 (s, 1C, C^b), 129.6 (s, 1C, C$^{3'}$), 127.7 (s, 1C, C^e), 125.7 (s, 1C, C^d), 124.2 (s, 1C, C^f), 123.2 (s, 1C, C$^{6'}$), 122.5 (s, 1C, C^c), 120.6 (s, 1C, C$^{2'}$), 116.0 (s, 1C, C$^{4'}$), 103.3 (s, 1C, C^1), 98.5 (s, 1C, C^4), 83.6 (s, 1C, C^2 or C^6), 82.3 (s, 1C, C^6 or C^2), 82.1 (s, 1C, C^3 or C^5), 81.5 (s, 1C, C^5 or C^3), 30.5 (s, 1C, C^7), 22.2 (s, 1C, C^8 or C^9), 21.2 (s, 1C, C^9 or C^8), 18.1 (s, 1C, C^{10}) ppm. **FT-IR (KBr, cm^{-1}) selected bands**: 3036 (w, $\nu_{=CH}$), 2962 (w, ν_{-CH}), 2090 (vs, $\nu_{C-N(SCN)}$), 1598 (s, ν_{C-N}), 1543 (s, $\nu_{C=C}$), 1489 (vs, $\nu_{C=N}$), 1455 (s), 1442 (s), 1419 (m), 1336 (s), 1212 (s, ν_{C-O}), 1152 (s, $\nu_{C=S}$), 1130 (w), 1032 (w), 877 (w), 836 (w), 819 (w), 751 (vs, $\nu_{C-S(SCN)}$), 726 (w). **MS (FAB+)**: m/z (%) = 982 (2) ([2M-NCS]$^+$), 462 (100) ([M-NCS]$^+$). **Molar Conductivity (CH_3CN)**: 1.9 S cm^2 mol^{-1}. **Solubility**: soluble in chloroform, acetonitrile, and dimethyl sulfoxide; partially soluble in methanol and insoluble in water and acetone.

Synthesis of [(η^6-Benzene)Ru(NCS)(κ^2-O,N-L2)], [3b]. The synthesis was performed as for [**3a**] in the presence of the ligand 2-(2′-hydroxyphenyl)benzothiazole (0.0911 g, 0.400 mmol), $[RuCl_2(bz)]_2$ (0.1002 g, 0.200 mmol), Et_3N (59 μL, 0.424 mmol), and KSCN (0.053 g, 0.545 mmol) in methanol (8 mL). Orange powder. Yield: 113.7 mg (0.245 mmol, 62%). **M$_r$ ($C_{20}H_{14}N_2ORuS_2$)** = 463.5454 g/mol. **Anal. Calc. for $C_{20}H_{14}N_2ORuS_2{\cdot}(CH_3CN)_{0.25}{\cdot}(H_2O)$**: C 50.06; H 3.43; N 6.41; S 13.04 **Found**: C 50.20; H 3.48; N 6.08; S 12.61. **^{1}H NMR (400 MHz, CD_2Cl_2, 25 °C)** δ 8.24 (d, J = 8.4 Hz, 1H, H^f), 7.91 (d, J = 8.0 Hz, 1H, H^c), 7.68 (ddd, J = 8.4, 7.2, 1.2 Hz, 1H, H^e), 7.56 (dd, J = 7.9, 1.7 Hz, 1H, H$^{3'}$), 7.51 (ddd, J = 8.4, 7.3, 1.1 Hz, 1H, H^d), 7.33 (ddd, J = 8.7, 7.0, 1.7 Hz, 1H, H$^{5'}$), 7.17 (dd, J = 8.4, 1.2 Hz, 1H, H$^{6'}$), 6.69 (ddd, J = 8.1, 7.0, 1.1 Hz, 1H, H$^{4'}$), 5.64 (s, 6H, H^{bz}) ppm. **FT-IR (KBr, cm^{-1}) selected bands**: 3055 (w, $\nu_{=CH}$), 3000 (w, $\nu_{=CH}$), 2099 (vs, $\nu_{C-N(SCN)}$), 1597 (s, ν_{C-N}), 1543 (m, $\nu_{C=C}$), 1494 (s, $\nu_{C=N}$), 1456 (s), 1439 (s), 1420 (m), 1332 (m), 1238 (m), 1223−1210 (s, ν_{C-O}), 1149 (m, $\nu_{C=S}$), 1125 (w), 1036−1016 (w), 982 (w), 834 (m), 813 (w), 750 (s, $\nu_{C-S(SCN)}$), 724 (w). **MS (FAB+)**: m/z (%) = 406 (7) ([M-NCS]$^+$) **Molar Conductivity**: It could not be measured due to their poor solubility. **Solubility**: partially soluble in dichloromethane. Slightly soluble in chloroform, methanol, dimethyl sulfoxide, acetonitrile, benzene, and acetone; insoluble in water.

■ ASSOCIATED CONTENT

Supporting Information

The Supporting Information is available free of charge on the ACS Publications website at DOI: 10.1021/acs.inorgchem.8b02299.

X-ray crystallographic files in CIF format; tables and figures with information on molecular and crystalline structures, ^{1}H NMR spectra, photo physical studies of compounds in solution and in presence of DNA, FAB-MS spectra, cleavage electrophoresis (PDF)

Accession Codes

CCDC 1815683−1815686 contain the supplementary crystallographic data for this paper. These data can be obtained free of charge via www.ccdc.cam.ac.uk/data_request/cif, or by emailing data_request@ccdc.cam.ac.uk, or by contacting The Cambridge Crystallographic Data Centre, 12 Union Road, Cambridge CB2 1EZ, UK; fax: +44 1223 336033.

■ AUTHOR INFORMATION

Corresponding Authors

*E-mail: nbusto@ubu.es.
*E-mail: gespino@ubu.es.
*E-mail: begar@ubu.es.

ORCID

Marta Martínez-Alonso: 0000-0002-0931-5274
Natalia Busto: 0000-0001-9637-1209
Blanca R. Manzano: 0000-0002-4908-4503
José L. Albasanz: 0000-0002-9927-5076
Gustavo Espino: 0000-0001-5617-5705
Begoña García: 0000-0002-0817-1651

Author Contributions

¶M.L. and M.M.-A. have contributed equally to the realization of this work.

Notes

The authors declare no competing financial interest.

■ ACKNOWLEDGMENTS

The financial support by "la Caixa" Foundation ((LCF/PR/PR12/11070003), MINECO (CTQ2014-58812-C2-2-R and CTQ2014-58812-C2-1-R FEDER Funds), and Junta de Castilla y León and Fondo Social Europeo (BU042U16), Spain, is gratefully acknowledged.

■ REFERENCES

(1) Rosenberg, B.; Van Camp, L.; Krigas, T. Inhibition of Cell Division in *Escherichia coli* by Electrolysis Products from a Platinum Electrode. *Nature* **1965**, *205*, 698−699.

(2) Ho, Y.-P.; Au-Yeung, S. C. F.; To, K. K. W. Platinum-based anticancer agents: innovative design strategies and biological perspectives. *Med. Res. Rev.* **2003**, *23*, 633−655.

(3) Levina, A.; Mitra, A.; Lay, P. A. Recent developments in ruthenium anticancer drugs. *Metallomics* **2009**, *1*, 458−470.

DOI: 10.1021/acs.inorgchem.8b02299
Inorg. Chem. XXXX, XXX, XXX−XXX

(4) Medici, S.; Peana, M.; Nurchi, V. M.; Lachowicz, J. I.; Crisponi, G.; Zoroddu, M. A. Noble metals in medicine: latest advances. *Coord. Chem. Rev.* **2015**, *284*, 329−350.
(5) Blunden, B. M.; Stenzel, M. H. Incorporating ruthenium into advanced drug delivery carriers − an innovative generation of chemotherapeutics. *J. Chem. Technol. Biotechnol.* **2015**, *90*, 1177−1195.
(6) Reisner, E.; Arion, V. B.; Keppler, B. K.; Pombeiro, A. J. L. Electron-transfer activated metal-based anticancer drugs. *Inorg. Chim. Acta* **2008**, *361*, 1569−1583.
(7) Scolaro, C.; Chaplin, A. B.; Hartinger, C. G.; Bergamo, A.; Cocchietto, M.; Keppler, B. K.; Sava, G.; Dyson, P. J. Tuning the hydrophobicity of ruthenium(II)−arene (RAPTA) drugs to modify uptake, biomolecular interactions and efficacy. *Dalton Trans.* **2007**, *2*, 5065−5072.
(8) Bruijnincx, P. C. A.; Sadler, P. J. Controlling Platinum, Ruthenium, and Osmium Reactivity for Anticancer Drug Design. *Adv. Inorg. Chem.* **2009**, *61*, 1−62.
(9) Peacock, A. F. A.; Sadler, P. J. Medicinal organometallic chemistry: designing metal arene complexes as anticancer agents. *Chem. - Asian J.* **2008**, *3*, 1890−1899.
(10) Pizarro, A. M.; Habtemariam, A.; Sadler, P. J. *Medicinal Organometallic Chemistry*; Springer: Berlin, Heidelberg, Germany, 2010; pp 21−56.
(11) Wang, H.-Y.; Qian, Y.; Wang, F.-X.; Habtemariam, A.; Mao, Z.-W.; Sadler, P. J.; Liu, H.-K. Ruthenium(II)−Arene Metallacycles: Crystal Structures, Interaction with DNA, and Cytotoxicity. *Eur. J. Inorg. Chem.* **2017**, *12*, 1792−1799.
(12) Singh, S. K.; Pandey, D. S. Multifaceted half-sandwich arene−ruthenium complexes: interactions with biomolecules, photoactivation, and multinuclearity approach. *RSC Adv.* **2014**, *4*, 1819−1840.
(13) Süss-Fink, G. Arene ruthenium complexes as anticancer agents. *Dalton Trans.* **2010**, *39*, 1673−1688.
(14) Akhtar, T.; Hameed, S.; Al-Masoudi, N.; Loddo, R.; Colla, P. In vitro antitumor and antiviral activities of new benzothiazole and 1,3,4-oxadiazole-2-thione derivatives. *Acta Pharm.* **2008**, *58*, 135−149.
(15) Chaudhary, P.; Sharma, K.; Sharma, A.; Varshney, J. Recent advances in pharmacological activity of benzothiazole derivatives. *Int. J. Curr. Pharm. Res.* **2010**, *2*, 5−11.
(16) Zimmermann, G.; Papke, B.; Ismail, S.; Vartak, N.; Chandra, A.; Hoffmann, M.; Hahn, S. A.; Triola, G.; Wittinghofer, A.; Bastiaens, P. I. H.; Waldmann, H. *Nature* **2013**, *497*, 638−642.
(17) Ginzinger, W.; Mühlgassner, G.; Arion, V. B.; Jakupec, M. A.; Roller, A.; Galanski, M.; Reithofer, M.; Berger, W.; Keppler, B. K. A SAR study of novel antiproliferative ruthenium and osmium complexes with quinoxalinone ligands in human cancer cell lines. *J. Med. Chem.* **2012**, *55*, 3398−3413.
(18) Yellol, G. S.; Donaire, A.; Yellol, J. G.; Vasylyeva, V.; Janiak, C.; Ruiz, J. On the antitumor properties of novel cyclometalated benzimidazole Ru(II), Ir(III) and Rh(III) complexes. *Chem. Commun.* **2013**, *49*, 11533−11535.
(19) Kottukulam Subran, S.; Banerjee, S.; Mondal, A.; Paira, P. Amberlite IR-120(H)-mediated "on water" synthesis of novel anticancer ruthenium(II)−*p*-cymene 2-pyridinylbenzothiazole (BTZ), 2-pyridinylbenzoxazole (BOZ) & 2-pyridinylbenzimidazole (BIZ) scaffolds. *New J. Chem.* **2016**, *40*, 10333−10343.
(20) Spillane, C. B.; Fletcher, N. C.; Rountree, S. M.; van den Berg, H.; Chanduloy, S.; Morgan, J. L.; Keene, F. R. Benzothiazole bipyridine complexes of ruthenium(II) with cytotoxic activity. *J. Biol. Inorg. Chem.* **2007**, *12*, 797−807.
(21) Ong, J. X.; Yap, C. W.; Ang, W. H. Rational design of selective organoruthenium Inhibitors of Protein Tyrosine Phosphatase. *Inorg. Chem.* **2012**, *51*, 12483−12492.
(22) Yellol, G. S.; Yellol, J. G.; Kenche, V. B.; Liu, X. M.; Barnham, K. J.; Donaire, A.; Janiak, C.; Ruiz, J. Synthesis of 2-pyridyl-benzimidazole iridium(III), ruthenium(II), and platinum(II) complexes. Study of the activity as inhibitors of amyloid-β aggregation and neurotoxicity evaluation. *Inorg. Chem.* **2015**, *54*, 470−475.
(23) Spillane, C. B.; Morgan, J. L.; Fletcher, N. C.; Collins, J. G.; Keene, F. R. Inert benzothiazole functionalised ruthenium(II) complexes; potential DNA hairpin binding agents. *Dalton Trans.* **2006**, 3122−3133.
(24) Spillane, C. B.; Dabo, M. N. V.; Fletcher, N. C.; Morgan, J. L.; Keene, F. R.; Haq, I.; Buurma, N. J. The Dichotomy in the DNA-Binding Behaviour of Ruthenium(II) Complexes Bearing Benzoxazole and Benzothiazole Groups. *J. Inorg. Biochem.* **2008**, *102*, 673−683.
(25) Martínez-Alonso, M.; Busto, N.; Jalón, F. A.; Manzano, B. R.; Leal, J. M.; Rodríguez, A. M.; García, B.; Espino, G. Derivation of Structure−Activity Relationships from the Anticancer Properties of Ruthenium(II) Arene Complexes with 2-Aryldiazole Ligands. *Inorg. Chem.* **2014**, *53*, 11274−11288.
(26) Smith, N. A.; Sadler, P. J. Philos. Trans. A. Photoactivatable metal complexes: from theory to applications in biotechnology and medicine. *Philos. Trans. R. Soc., A* **2013**, *371*, 20120519.
(27) Lameijer, L. N.; Ernst, D.; Hopkins, S. L.; Meijer, M. S.; Askes, S. H. C.; Le Dévédec, S. E.; Bonnet, S. A Red-Light-Activated Ruthenium-Caged NAMPT Inhibitor Remains Phototoxic in Hypoxic Cancer Cells. *Angew. Chem., Int. Ed.* **2017**, *56*, 11549−11553.
(28) Qu, F.; Park, S.; Martinez, K.; Gray, J. L.; Thowfeik, F. S.; Lundeen, J. A.; Kuhn, A. E.; Charboneau, D. J.; Gerlach, D. L.; Lockart, M. M.; Law, J. A.; Jernigan, K. L.; Chambers, N.; Zeller, M.; Piro, N. A.; Kassel, W. S.; Schmehl, R. H.; Paul, J. J.; Merino, E. J.; Kim, Y.; Papish, E. T. Ruthenium Complexes are pH-Activated Metallo Prodrugs (pHAMPs) with Light-Triggered Selective Toxicity Toward Cancer Cells. *Inorg. Chem.* **2017**, *56*, 7519−7532.
(29) Zeng, L.; Gupta, P.; Chen, Y.; Wang, E.; Ji, L.; Chao, H.; Chen, Z.-S. The development of anticancer ruthenium(ii) complexes: from single molecule compounds to nanomaterials. *Chem. Soc. Rev.* **2017**, *46*, 5771−5804.
(30) White, J. K.; Schmehl, R. H.; Turro, C. An Overview Of Photosubstitution Reactions Of Ru(II) Imine Complexes And Their Application In Photobiology And Photodynamic Therapy. *Inorg. Chim. Acta* **2017**, *454*, 7−20.
(31) Brabec, V.; Pracharova, J.; Stepankova, J.; Sadler, P. J.; Kasparkova, J. Photo-induced DNA cleavage and cytotoxicity of a ruthenium(II) arene anticancer complex. *J. Inorg. Biochem.* **2016**, *160*, 149−155.
(32) Iglesias, R. S.; Gonçalves, P. F. B.; Livotto, P. R. Semiempirical study of a set of 2-(2′-hydroxyphenyl)benzazoles using the polarizable continuum model. *Chem. Phys. Lett.* **2000**, *327*, 23−28.
(33) Tong, Y.-P.; Zheng, S.-L.; Chen, X.-M. Structures, photoluminescence and theoretical studies of two Zn(II) complexes with substituted 2-(2-hydroxyphenyl)benzimidazoles. *Eur. J. Inorg. Chem.* **2005**, *2005*, 3734−3741.
(34) Tong, Y.-P.; Zheng, S.-L. Synthesis, structure, spectroscopic properties, DFT and TDDFT investigations of copper(II) complex with 2 -(2-hydroxyphenyl)benzimidazole. *J. Mol. Struct.* **2007**, *841*, 34−40.
(35) Rodríguez-Rodríguez, C.; Sánchez de Groot, N.; Rimola, A.; Álvarez-Larena, A.; Lloveras, V.; Vidal-Gancedo, J.; Ventura, S.; Vendrell, J.; Sodupe, M.; González-Duarte, P. Design, selection, and characterization of thioflavin-based intercalation compounds with metal chelating properties for application in Alzheimer's disease. *J. Am. Chem. Soc.* **2009**, *131*, 1436−1451.
(36) Mandal, S. K.; Chakravarty, A. R. Diasteroisomeric (η^6arene)-ruthenium(II) chiral Schiff base complexes: crystal structure of a triphenylphosphine adduct. *J. Organomet. Chem.* **1991**, *417*, C59−C62.
(37) Ganter, C. Chiral organometallic half-sandwich complexes with defined metal configuration. *Chem. Soc. Rev.* **2003**, *32*, 130−138.
(38) Kargol, J. A.; Crecely, R. W.; Burmeister, J. L. Carbon-13 nuclear magnetic resonance study of coordinated thiocyanate, selenocyanate, and cyanate. *Inorg. Chem.* **1979**, *18*, 2532−2535.
(39) Nakamoto, K.; Nakamoto, K. *Infrared and Raman Spectra of Inorganic and Coordination Compounds. Part A: Theory and Applications in Inorganic Chemistry*; Wiley: Weinheim, Germany, 2009.

DOI: 10.1021/acs.inorgchem.8b02299
Inorg. Chem. XXXX, XXX, XXX−XXX

(40) Campos, J.; Álvarez, E.; Carmona, E. Synthesis and reactivity of half-sandwich (η^5-C_5Me_5)Ir(III) complexes of a cyclometallated aryl phosphine ligand. *New J. Chem.* **2011**, *35*, 2122−2129.
(41) Vandenburgh, L.; Buck, M. R.; Freedman, D. A. Preparation, separation, and characterization of ruthenium(II) thiocyanate linkage isomers. *Inorg. Chem.* **2008**, *47*, 9134−9136.
(42) Geary, W. J. The use of conductivity measurements in organic solvents for the characterisation of coordination compounds. *Coord. Chem. Rev.* **1971**, *7*, 81−122.
(43) Constable, E. C.; Housecroft, C. E.; Schneider, G. E.; Zampese, J. A. A homage to Alfred Werner: Exploring the stereochemical complexity of cyclometallated $[Ir(ppy)_2XY]^{n+}$ complexes (Hppy = 2-phenylpyridine). *Polyhedron* **2013**, *52*, 530−537.
(44) Pérez-García, L.; Amabilino, D. B. Spontaneous resolution under supramolecular control. *Chem. Soc. Rev.* **2002**, *31*, 342−356.
(45) Steed, J. W.; Tocher, D. A. Geometrical isomerism in 2-hydroxypyridinate and pyridine-2-thiolate complexes derived from the ruthenium(IV) bis(allyl) dimer $[\{Ru(\eta^3:\ \eta^3\text{-}C_{10}H_{16})Cl(\mu\text{-}Cl)\}_2]$. *J. Chem. Soc., Dalton Trans.* **1992**, 2765−2773.
(46) Chakrabarti, P.; Bhattacharyya, R. Geometry of nonbonded interactions involving planar groups in proteins. *Prog. Biophys. Mol. Biol.* **2007**, *95*, 83−137.
(47) Reid, K. S. C.; Lindley, P. F.; Thornton, J. M. Sulphur-aromatic interactions in proteins. *FEBS Lett.* **1985**, *190*, 209−213.
(48) Kim, T.-I.; Kang, H. J.; Han, G.; Chung, S. J.; Kim, Y. A highly selective fluorescent ESIPT probe for the dual specificity phosphatase MKP-6. *Chem. Commun.* **2009**, 5895−5897.
(49) Habtemariam, A.; Melchart, M.; Fernández, R.; Parsons, S.; Oswald, I. D. H.; Parkin, P.; Fabbiani, F.; Davidson, J. E.; Dawson, A.; Aird, R. E.; Jodrell, D. I.; Sadler, P. J. Structure−Activity Relationships for Cytotoxic Ruthenium(II) Arene Complexes Containing N,N-, N,O-, and O,O-Chelating Ligands. *J. Med. Chem.* **2006**, *49*, 6858−6868.
(50) Wang, F.; Habtemariam, A.; van der Geer, E. P. L.; Fernández, R.; Melchart, M.; Deeth, R. J.; Aird, R.; Guichard, S.; Fabbiani, F. P. A.; Lozano-Casal, P.; Oswald, I. D. H.; Jodrell, D. I.; Parsons, S.; Sadler, P. J. Controlling ligand substitution reactions of organometallic complexes: Tuning cancer cell cytotoxicity. *Proc. Natl. Acad. Sci. U. S. A.* **2005**, *102*, 18269−18274.
(51) Po, H. N.; Senozan, N. M. Controlling ligand substitution reactions of organometallic complexes: Tuning cancer cell cytotoxicity. *J. Chem. Educ.* **2001**, *78*, 1499−1503.
(52) Dey, J.; Dogra, S. K. Electronic absorption and fluorescence spectra of 2-phenyl-substituted benzothiazoles: study of excited-state proton transfer reactions. *Can. J. Chem.* **1991**, *69*, 1539−1547.
(53) Ren, J.; Chaires, J. B. Sequence and Structural Selectivity of Nucleic Acid Binding Ligands. *Biochemistry* **1999**, *38*, 16067−16075.
(54) Neidle, S. DNA minor-groove recognition by small molecules. *Nat. Prod. Rep.* **2001**, *18*, 291−309.
(55) Suter, B.; Schnappauf, G.; Thoma, F. Poly(dA·dT) sequences exist as rigid DNA structures in nucleosome-free yeast promoters in vivo. *Nucleic Acids Res.* **2000**, *28*, 4083−4089.
(56) Chen, H.; Parkinson, J. A.; Parsons, S.; Coxall, R. A.; Gould, R. O.; Sadler, P. J. Organometallic Ruthenium(II) Diamine Anticancer Complexes: Arene-Nucleobase Stacking and Stereospecific Hydrogen-Bonding in Guanine Adducts. *J. Am. Chem. Soc.* **2002**, *124*, 3064−3082.
(57) Yan, Y. K.; Melchart, M.; Habtemariam, A.; Sadler, P. J. Organometallic chemistry, biology and medicine: ruthenium arene anticancer complexes. *Chem. Commun.* **2005**, 4764−4776.
(58) García, B.; Garcia-Tojal, J.; Ruiz, R.; Gil-García, R.; Ibeas, S.; Donnadieu, B.; Leal, J. M. Binding of the DNA bases and their mononucleotides to pyridine-2-carbaldehyde thiosemicarbazonecopper(II) complexes. Structure of the cytosine derivative. *J. Inorg. Biochem.* **2008**, *102*, 1892−1900.
(59) Friedman, A. E.; Chambron, J. C.; Sauvage, J. P.; Turro, N. J.; Barton, J. K. A molecular light switch for DNA: $Ru(bpy)2(dppz)^{2+}$. *J. Am. Chem. Soc.* **1990**, *112*, 4960−4962.
(60) Sun, Y.; Lutterman, D. A.; Turro, C. Role of Electronic Structure on DNA Light-Switch Behavior of Ru(II) Intercalators. *Inorg. Chem.* **2008**, *47*, 6427−6434.
(61) Busto, N.; Valladolid, J.; Martínez-Alonso, M.; Lozano, H. J.; Jalón, F. A.; Manzano, B. R.; Rodríguez, A. M.; Carrión, M. C.; Biver, T.; Leal, J. M.; Espino, G.; García, B. Anticancer Activity and DNA Binding of a Bifunctional Ru(II) Arene Aqua-Complex with the 2,4-Diamino-6-(2-pyridyl)-1,3,5-triazine ligand. *Inorg. Chem.* **2013**, *52*, 9962−9974.
(62) Magennis, S. W.; Habtemariam, A.; Novakova, O.; Henry, J. B.; Meier, S.; Parsons, S.; Oswald, I. D. H.; Brabec, V.; Sadler, P. J. Dual Triggering of DNA Binding and Fluorescence via Photoactivation of a Dinuclear Ruthenium(II) Arene Complex. *Inorg. Chem.* **2007**, *46*, 5059−5068.
(63) Weber, W.; Ford, P. C. Photosubstitution reactions of the ruthenium(II) arene complexes Ru(.eta.6-arene)L32+ (L = ammonia or water) in aqueous solution. *Inorg. Chem.* **1986**, *25*, 1088−1092.
(64) Barragán, F.; López-Senín, P.; Salassa, L.; Betanzos-Lara, S.; Habtemariam, A.; Moreno, V.; Sadler, P. J.; Marchán, V. Photocontrolled DNA Binding of a Receptor-Targeted Organometallic Ruthenium(II) Complex. *J. Am. Chem. Soc.* **2011**, *133*, 14098−14108.
(65) Presa, A.; Brissos, R. F.; Caballero, A. B.; Borilovic, I.; Korrodi-Gregório, L.; Pérez-Tomás, R.; Roubeau, O.; Gamez, P. Photoswitching the Cytotoxic Properties of Platinum(II) Compounds. *Angew. Chem.* **2015**, *127*, 4644−4648.
(66) Bennett, M. A.; Smith, A. K. Arene ruthenium(II) complexes formed by dehydrogenation of cyclohexadienes with ruthenium(III) trichloride. *J. Chem. Soc., Dalton Trans.* **1974**, 233−241.
(67) Brun, A. M.; Harriman, A. Energy- and Electron-Transfer Processes Involving Palladium Porphyrins Bound to DNA. *J. Am. Chem. Soc.* **1994**, *116*, 10383−10393.
(68) Fulmer, G. R.; Miller, A. J. M.; Sherden, N. H.; Gottlieb, H. E.; Nudelman, A.; Stoltz, B. M.; Bercaw, J. E.; Goldberg, K. I. NMR Chemical Shifts of Trace Impurities: Common Laboratory Solvents, Organics, and Gases in Deuterated Solvents Relevant to the Organometallic Chemist. *Organometallics* **2010**, *29*, 2176−2179.
(69) Cohen, G.; Eisenberg, H. Viscosity and sedimentation study of sonicated DNA−proflavine complexes. *Biopolymers* **1969**, *8*, 45−55.
(70) Liu, Y. S.; Zeng, C. H.; Huang, H. L.; He, L. X.; Wu, F. H. Synthesis, DNA-binding, photocleavage, cytotoxicity and antioxidant activity of ruthenium (II) polypyridyl complexes. *Eur. J. Med. Chem.* **2010**, *45*, 564−571.
(71) Neves, A.; Terenzi, H.; Horner, R.; Horn, A., Jr; Szpoganicz, B.; Sugai, J. Hydrolytic DNA cleavage promoted by a dinuclear iron (III) complex. *Inorg. Chem. Commun.* **2001**, *4*, 388−391.
(72) *SAINT v8.37, APEX3 v2016.1.0*; Bruker-AXS: Madison, WI, 2016.
(73) SADABS: Krause, L.; Herbst-Irmer, R.; Sheldrick, G. M.; Stalke, D. Comparison of silver and molybdenum microfocus X-ray sources for single-crystal structure determination. *J. Appl. Crystallogr.* **2015**, *48*, 3−10.
(74) (a) Farrugia, L. J. WinGX and ORTEP for Windows: an update. *J. Appl. Crystallogr.* **2012**, *45*, 849−854. (b) . Sheldrick, G. M. *SHELX-2014, Program for Crystal Structure Refinement*; University of Göttingen: Göttingen, Germany, 2014.

DOI: 10.1021/acs.inorgchem.8b02299
Inorg. Chem. XXXX, XXX, XXX−XXX